Precambrian Research 245 (2014) 13–28

Contents lists available at ScienceDirect

Precambrian Research

journal homepage: www.elsevier.com/locate/precamres

Neoproterozoic subduction along the Ailaoshan zone, South China: Geochronological and geochemical evidence from amphibolite

Yongfeng Cai[a,b,c], Yuejun Wang[b,d,*], Peter A. Cawood[e,f], Weiming Fan[g], Huichuan Liu[a,c], Xiaowan Xing[a,c], Yuzhi Zhang[a]

[a] State Key Laboratory of Isotope Geochemistry, Guangzhou Institute of Geochemistry, Chinese Academy of Sciences, Guangzhou 510640, China
[b] Department of Earth Sciences, Sun Yat-Sen University, Guangzhou 510275, China
[c] University of Chinese Academy of Sciences, Beijing 100049, China
[d] Guangdong Provincial Key Laboratory of Mineral Resources and Geological Processes, Guangzhou 510275, China
[e] Department of Earth Sciences, University of St Andrews, North Street, St Andrews KY16 9AL, UK
[f] School of Earth and Environment, University of Western Australia, 35 Stirling Highway, Crawley, WA 6009, Australia
[g] Key Laboratory of Continental Collision and Plateau Uplift, Institute of Tibetan Plateau Research, Chinese Academy of Sciences, Beijing 100101, China

ARTICLE INFO

Article history:
Received 28 October 2013
Received in revised form 22 January 2014
Accepted 24 January 2014
Available online 1 February 2014

Keywords:
Ailaoshan zone
Amphibolite
Zircon U–Pb dating
Petrogenesis
Neoproterozoic subduction

ABSTRACT

Lenses of amphibolites occur along the Ailaoshan suture zone at the southwestern margin of the Yangtze Block, South China. Petrological, geochemical and zircon U–Pb geochronological data indicate that they are divisible into two coeval groups. Group 1, represented by the Jinping amphibolite, has mg-number of 71–76 and (La/Yb)cn ratios of 7.2–7.7, and displays a geochemical affinity to island arc volcanic rocks. Group 2 amphibolites occur at Yuanyang and are characterized by high Nb contents (14.3–18.4 ppm), resembling Nb-enriched basalts. The $\varepsilon_{Nd}(t)$ values for Group 1 range from −3.45 to −2.04 and for Group 2 from +4.08 to +4.39. A representative sample for Group 1 yields a U–Pb zircon age of 803 ± 7 Ma, whereas two samples for Group 2 give U–Pb zircon ages of 813 ± 11 Ma and 814 ± 12 Ma. Petrogenetic analysis suggests that Group 1 originated from an orthopyroxene-rich source and Group 2 from a mantle wedge modified by slab-derived melt. In combination with other geological observations, these amphibolites are inferred to constitute part of an early Neoproterozoic (~815–800 Ma) arc-back-arc basin system. The Neoproterozoic amphibolites and related rocks along the Ailaoshan zone may be the southward extension of the Neoproterozoic supra-subduction zone that developed along the western margin of the Yangtze Block.

1. Introduction

The position of South China Craton (SCC) has played a key role in paleogeographic models for assembly of Precambrian supercontinents and contrasting intracratonic and peripheral locations have been proposed (e.g., Cawood et al., 2013; Li et al., 1995, 2008a; Yan et al., 2004; Zhao and Cawood, 1999; Zhao and Guo, 2012; Zhou et al., 2002a). Key to resolving this controversy is to understand the tectonic setting of Neoproterozoic igneous rocks within the SCC, and whether they formed in supra-subduction zone and/or within-plate environments. These Neoproterozoic igneous rocks are mainly distributed along the northern, western and eastern margins of the Yangtze Block and their petrogenesis and tectonic environment has been a focus of intense study and debate (e.g., Chen et al., 2013; Dong et al., 2011, 2012; Li et al., 2002, 2003a; Zhang et al., 2013b; Zhao and Cawood, 2012; Zhao et al., 2011; Zhou et al., 2002a, 2006b). In this study, we document the petrological characteristics, geochemical affinities and tectonic setting of the newly-identified Neoproterozoic amphibolites along the Ailaoshan zone adjacent to the southwestern margin of the Yangtze Block. These data indicate a supra-subduction zone setting and constrain the Neoproterozoic location of South China to a position along the northern margin of the Rodinia supercontinent.

2. Geological setting

The Ailaoshan suture zone forms part of a major tectonic zone that marks the southern boundary of the SCC (Fig. 1). It can be traced for at least 300 km and is up to 30 km wide in Yunnan Province, SW China. The zone was reactivated in the late Paleozoic to early Mesozoic during closure of the Tethys Ocean and resultant accretion of the Indochina Block to the southeast of the suture zone (e.g., Charvet et al., 1996; Zhong, 1998). Subsequent strike-slip

* Corresponding author at: Department of Earth Sciences, Sun Yat-Sen University, No. 135, Xingang Xi Road, Guangzhou 510275, China. Tel.: +86 20 84111209; fax: +86 20 84111209.
E-mail address: wangyuejun@mail.sysu.edu.cn (Y. Wang).

0301-9268/$ – see front matter © 2014 Elsevier B.V. All rights reserved.
http://dx.doi.org/10.1016/j.precamres.2014.01.009

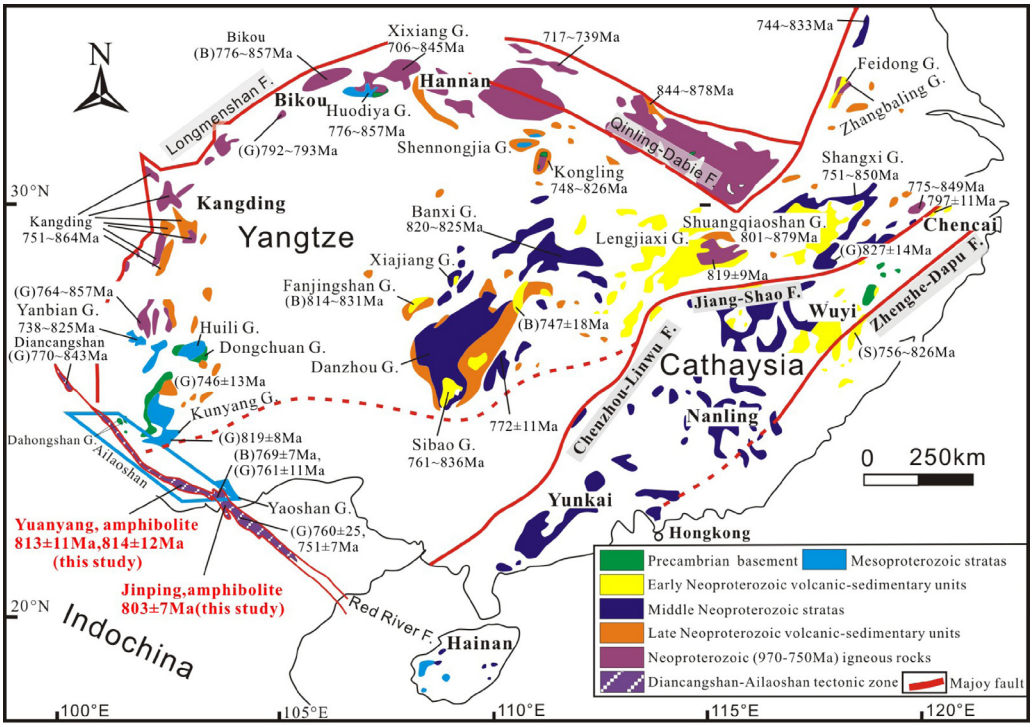

Fig. 1. Simplified geotectonic map showing the Ailaoshan zone (modified after Leloup et al., 1995; Lin et al., 2012; Zhao and Cawood, 2012). (G) and (B) refer to the ages for granite and basalt and others from the volcanics from the sedimentary-volcanic sequence. The cited geochronological data are from Supplementary Table 1.

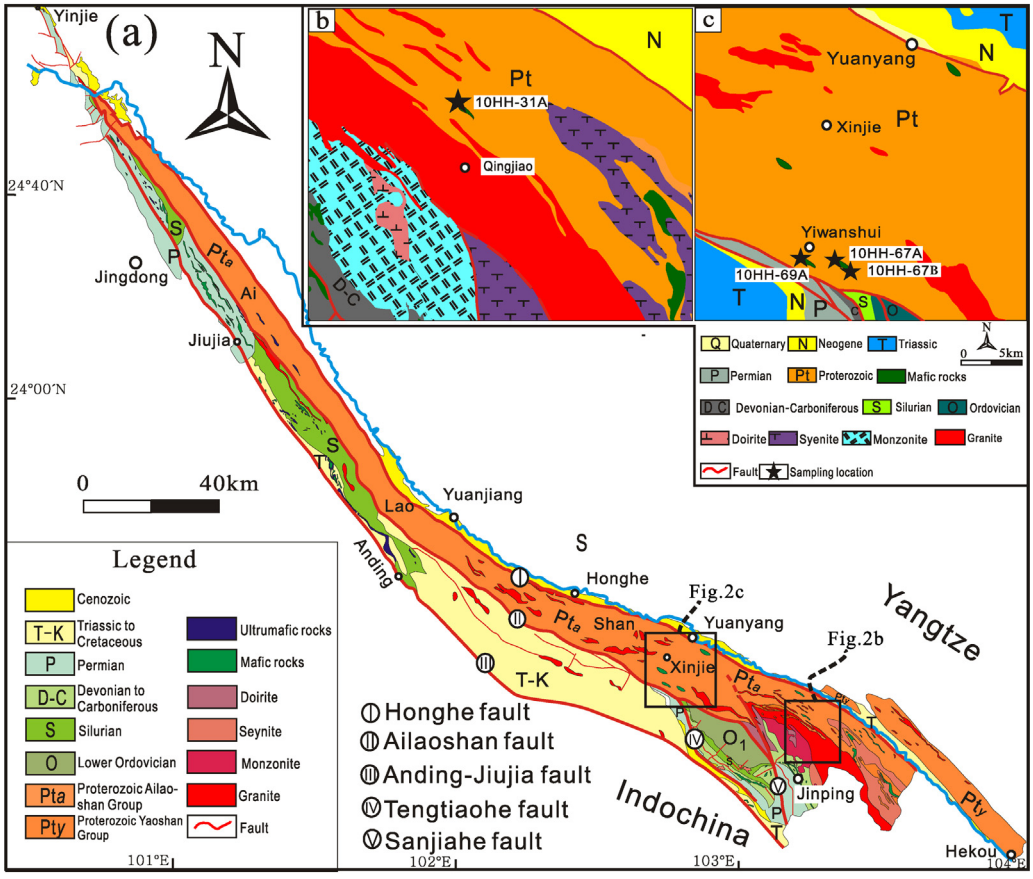

Fig. 2. (a) Schematic geological map of the Ailaoshan suture zone showing (b) the distribution of amphibolites at Jinping and (c) at Yuanyang.

Table 1
SIMS and LA-ICP-MS zircon U–Pb isotopic analyses of the representative amphibolites along the Ailaoshan zone.

Spot	Element (ppm)		Th/U	Isotope ratio						Age (Ma)			
	^{232}Th	^{238}U		^{207}Pb/^{206}Pb	±1σ	^{207}Pb/^{235}U	±1σ	^{206}Pb/^{238}U	±1σ	^{207}Pb/^{206}Pb	±1σ	^{206}Pb/^{238}U	±1σ
10HH-31A amphibolite, Qingjiao, Jinping in western Yunnan (LA-ICPMS dating method)													
10HH-31A-01	244	322	0.76	0.0655	0.002	1.1839	0.03	0.1311	0.003	790	48	794	15
10HH-31A-02	277	560	0.49	0.0647	0.002	0.9885	0.02	0.1108	0.002	765	57	677	14
10HH-31A-03	136	154	0.88	0.0759	0.004	1.3726	0.07	0.1311	0.005	1093	112	794	26
10HH-31A-04	252	369	0.68	0.0703	0.003	1.2151	0.04	0.1253	0.003	937	73	761	17
10HH-31A-05	238	326	0.73	0.0658	0.002	1.2238	0.03	0.1349	0.003	799	62	816	17
10HH-31A-06	536	504	1.07	0.0671	0.002	1.2264	0.03	0.1325	0.003	841	52	802	15
10HH-31A-07	268	332	0.81	0.0671	0.002	1.2660	0.04	0.1368	0.003	841	68	827	18
10HH-31A-08	558	1138	0.49	0.0660	0.001	1.2007	0.02	0.1320	0.002	805	39	799	14
10HH-31A-09	269	305	0.88	0.0668	0.002	1.2685	0.04	0.1377	0.003	832	68	832	18
10HH-31A-10	345	386	0.89	0.0649	0.002	1.1933	0.03	0.1334	0.003	770	52	807	15
10HH-31A-11	413	480	0.86	0.0644	0.002	1.1721	0.03	0.1321	0.003	753	56	800	16
10HH-31A-12	245	401	0.61	0.0686	0.002	1.2742	0.03	0.1348	0.003	885	51	815	15
10HH-31A-13	244	313	0.78	0.0686	0.003	1.2478	0.06	0.1320	0.004	885	101	800	22
10HH-31A-14	221	265	0.83	0.0683	0.003	1.2078	0.04	0.1282	0.003	879	75	778	17
10HH-31A-15	254	323	0.79	0.0710	0.003	1.2629	0.04	0.1291	0.003	957	74	783	18
10HH-31A-16	208	117	1.78	0.0706	0.004	1.2572	0.07	0.1293	0.004	944	121	784	25
10HH-31A-17	299	336	0.89	0.0630	0.003	1.2042	0.05	0.1388	0.004	708	89	838	20
10HH-31A-18	274	333	0.82	0.0679	0.002	1.2624	0.04	0.1350	0.003	865	65	816	17
10HH-31A-19	311	425	0.73	0.0655	0.002	1.1984	0.03	0.1328	0.003	791	54	804	15
10HH-31A-20	397	419	0.95	0.0700	0.002	1.2746	0.04	0.1321	0.003	929	61	800	16
10HH-31A-21	278	442	0.63	0.0667	0.002	1.2341	0.03	0.1343	0.003	829	56	812	16
10HH-31A-22	313	381	0.82	0.0665	0.002	1.2368	0.04	0.1351	0.003	821	66	817	17
10HH-31A-23	174	355	0.49	0.0689	0.002	1.2384	0.04	0.1304	0.003	897	66	790	17
10HH-31A-24	571	591	0.97	0.0661	0.001	1.1964	0.02	0.1314	0.002	810	46	796	14
10HH-67A amphibolite, Yiwanshui, Yuanyang in western Yunnan (SIMS dating method)													
10HH-67A-01	516	662	0.78	0.0633	1.02	0.9332	1.83	0.1069	1.52	719	22	655	9
10HH-67A-02	1332	1992	0.67	0.0471	2.98	0.1270	3.33	0.0196	1.50	54	69	125	2
10HH-67A-03	120	224	0.54	0.0668	1.41	1.0776	2.06	0.1170	1.50	832	29	713	10
10HH-67A-04	48	520	0.09	0.0691	1.81	1.2949	2.36	0.1359	1.50	902	37	821	12
10HH-67A-05	87	139	0.62	0.0519	2.29	0.3314	2.76	0.0463	1.53	281	52	292	4
10HH-67A-06	225	302	0.75	0.0493	5.39	0.0353	5.66	0.0052	1.75	162	121	33	1
10HH-67A-07	299	486	0.62	0.0566	2.48	0.6198	2.90	0.0794	1.50	476	54	493	7
10HH-67A-08	108	284	0.38	0.0649	0.87	1.2175	1.75	0.1360	1.52	772	18	822	12
10HH-67A-09	264	501	0.53	0.0666	0.74	1.2082	1.67	0.1316	1.50	825	15	797	11
10HH-67A-10	527	561	0.94	0.1273	0.42	5.7767	1.56	0.3292	1.51	2061	7	1834	24
10HH-67A-11	145	390	0.37	0.0658	0.74	1.2221	1.67	0.1347	1.50	800	15	815	11
10HH-67A-12	312	302	1.03	0.0637	0.97	1.0159	1.79	0.1157	1.50	732	20	706	10
10HH-67A-13	173	196	0.88	0.0647	1.13	1.0889	1.88	0.1220	1.50	766	24	742	11
10HH-67A-14	325	835	0.39	0.0723	0.51	1.2108	1.59	0.1215	1.50	994	10	739	10
10HH-67A-15	469	1238	0.38	0.0676	0.53	1.1006	1.60	0.1180	1.50	857	11	719	10
10HH-67A-16	3400	12,288	0.28	0.0466	0.82	0.0317	1.71	0.0049	1.50	31	20	32	0
10HH-67B amphibolite, Yiwanshui, Yuanyang in western Yunnan (LA-ICPMS dating method)													
10HH-67B-01	105	112	0.94	0.0672	0.002	1.1298	0.03	0.1219	0.003	856	58	741	18
10HH-67B-02	206	355	0.58	0.0781	0.002	1.7348	0.04	0.1610	0.004	1150	50	962	23
10HH-67B-03	71	156	0.45	0.0662	0.002	1.2276	0.03	0.1346	0.003	813	49	814	20
10HH-67B-04	542	901	0.60	0.0659	0.002	1.0001	0.03	0.1099	0.003	806	54	672	18
10HH-67B-05	229	191	1.20	0.0678	0.002	1.2577	0.03	0.1346	0.003	861	56	814	20
10HH-67B-06	88	293	0.30	0.0541	0.001	0.2888	0.01	0.0388	0.001	372	57	245	6
10HH-67B-07	55	566	0.10	0.0679	0.002	1.2599	0.03	0.1345	0.003	865	52	814	20
10HH-67B-08	144	178	0.81	0.0656	0.002	1.2153	0.03	0.1343	0.003	794	58	812	19
10HH-67B-09	149	485	0.31	0.0672	0.002	1.2513	0.03	0.1351	0.003	843	52	817	20
10HH-67B-10	380	416	0.91	0.1291	0.003	6.6491	0.17	0.3738	0.010	2087	44	2047	46
10HH-67B-11	211	891	0.24	0.0662	0.002	1.0456	0.03	0.1145	0.003	813	52	699	18
10HH-67B-12	108	323	0.33	0.0666	0.002	1.2377	0.03	0.1348	0.003	833	52	815	20
10HH-67B-13	426	634	0.67	0.0598	0.002	0.6995	0.03	0.0835	0.002	594	56	517	15
10HH-67B-14	79	117	0.67	0.0553	0.001	0.3733	0.01	0.0491	0.001	433	59	309	8
10HH-67B-15	72	152	0.47	0.0556	0.001	0.3795	0.01	0.0496	0.001	435	62	312	8
10HH-67B-16	323	393	0.82	0.0472	0.001	0.0354	0.00	0.0055	0.000	61	63	35	1
10HH-67B-17	57	155	0.36	0.0660	0.002	1.2220	0.03	0.1343	0.003	806	53	812	20
10HH-67B-18	294	1155	0.25	0.0734	0.002	1.3669	0.03	0.1351	0.003	1033	52	817	19
10HH-67B-19	332	539	0.62	0.1897	0.005	11.9528	0.30	0.4568	0.012	2740	41	2425	51
10HH-67B-20	416	593	0.70	0.0596	0.002	0.6629	0.02	0.0806	0.002	591	28	500	12
10HH-67B-21	84	182	0.46	0.0689	0.002	1.2766	0.03	0.1342	0.003	896	54	812	19
10HH-67B-22	199	708	0.28	0.0600	0.002	0.6005	0.02	0.0725	0.002	606	54	451	11
10HH-67B-23	83	179	0.46	0.0652	0.002	1.2045	0.03	0.1340	0.003	789	52	811	19
10HH-67B-24	108	372	0.29	0.0779	0.002	1.7808	0.05	0.1656	0.004	1146	50	988	23
10HH-67B-25	108	1013	0.11	0.0603	0.002	0.6357	0.02	0.0764	0.002	617	86	474	12
10HH-67B-26	230	1608	0.14	0.0640	0.002	0.8241	0.02	0.0933	0.002	743	54	575	14

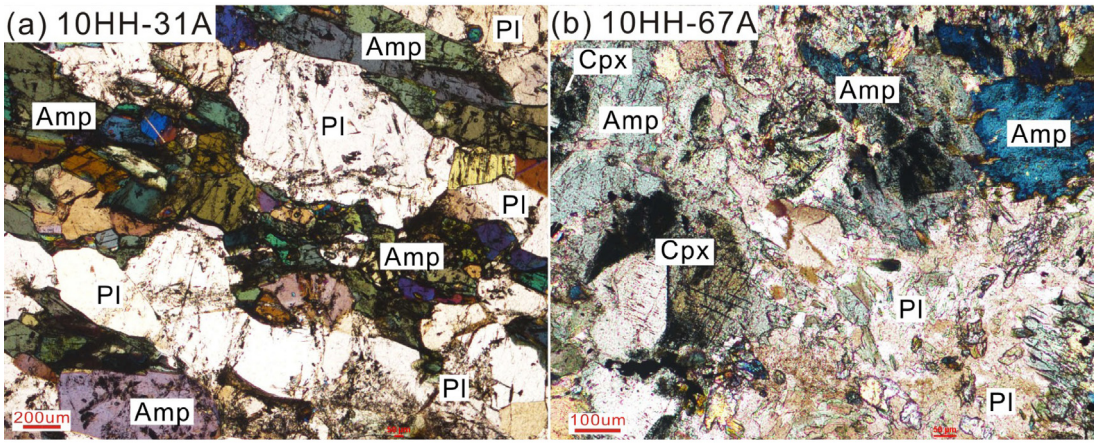

Fig. 3. Microscope photographs for the representative amphibolites along the Ailaoshan zone. (a) Amphibolite 10HH-31A, (b) amphibolite 10HH-67A. Amp: amphibole, Pl: plagioclase, Cpx: clinopyroxene.

deformation associated with the India-Asia collision during the Cenozoic period reactivated the Ailaoshan suture zone and further disrupted it into a series of faults, e.g., Red River, Ailaoshan, Jiujia-Anding, Lixiangjiang and Tengtiaohe faults (Fig. 2, e.g., Tapponnier et al., 1990).

The Cenozoic Ailaoshan Fault divides the suture zone into two lithotectonic successions (Fig. 2). To the northeast of the fault is a high-grade metamorphic succession of sillimanite-biotite gneiss, two-mica schist, amphibolite, biotite-amphibole-plagioclase gneiss, graphite-quartz marble, biotite gneiss, graphite schist, which together are defined as the Precambrian Ailaoshan Group/Complex (e.g., Lu, 1989; Yunnan BGMR, 1983; Zhong, 1998). To the southwest of the fault occurs a greenschist facies association of Paleozoic and earliest Mesozoic sedimentary and igneous rocks, including Permian ophiolitic fragments (Fan et al., 2010; Yunnan BGMR, 1983; Zhong, 1998). The Ailaoshan suture zone abuts the Yangtze Block (Figs. 1 and 2) that comprises Archean to Paleoproterozoic crystalline basement and Neoproterozoic to lower Paleozoic and upper Paleozoic marine packages (e.g., Cawood et al., 2013; Qiu et al., 2000; Wang et al., 2013a; Zhao and Cawood, 2012).

Within the Ailaoshan Group/Complex are small outcrops of mafic and ultramafic rocks that occur as lens, pods and isolated fragments. They consist mainly of hornblende pyroxenite, amphibolite and metagabbro, and peridotite and pyroxenite, and were previously considered to be Paleoproterozoic to Mesoproterozoic in age (e.g., Lu, 1989; Yunnan BGMR, 1983). Amphibolite is the dominant rock type and is the focus of this study. It is best developed in the Jinping and Yuanyang areas (Fig. 2b and c). The amphibolites at Jinping, named herein Group 1, show blastoporphyritic texture and banded structure and are composed of pleochroic hornblende (~40–50%), plagioclase (~30–45%), quartz (~5%), biotite (~3%) and small amounts of clinozoisite, chlorite, epidote, zircon, apatite and magnetite (Fig. 3a). The amphibolite at Yuanyang, named herein Group 2, display porphyroblastic texture and massive structure with the primary igneous textures often destroyed by later deformation and metamorphism. They consist of pleochroic hornblende (~50–60%), plagioclase (~20–30%), pyroxene (~3%), quartz (~3%), biotite (~2%) and small amounts of chlorite, epidote, magnetite, zircon and apatite (Fig. 3b).

3. Analytical methods

Zircon grains were extracted from three representative samples of amphibolites (10HH-67A, 10HH-31A and 10HH-67B) by conventional heavy liquid and magnetic techniques. These grains, together with zircon standard 91500, were mounted in epoxy. Transmitted and reflected light micrographs, along with cathodoluminescence (CL) images were taken to display the internal structure of all analyzed grains.

U–Th–Pb measurements for 10HH-67A were undertaken using the Cameca IMS-1280 SIMS at the Institute of Geology and Geophysics, Chinese Academy of Sciences (CAS). U–Th–Pb absolute abundances and ratios were determined relative to the standard zircon 91500 (Wiedenbeck et al., 1995). Detailed description of operating conditions and data processing procedures is given in Li et al. (2009a). The long-term uncertainty for $^{206}Pb/^{238}U$ measurements of the zircon standard of 1.5% (1 relative standard deviation, RSD) was propagated to the unknown zircons, although in our analytical sessions the measured $^{206}Pb/^{238}U$ error was usually about 1% (1 RSD) or less. Non-radiogenic ^{204}Pb was used for the common Pb correction. Corrections are sufficiently small to be insensitive to the choice of common Pb composition, and an average of present-day crustal composition (Stacey and Kramers, 1975) is used for the common Pb assuming that the common Pb is mainly due to surface contamination introduced during sample preparation. Uncertainties on individual analyses in data tables are reported at 1 sigma level and mean ages for pooled Pb/Pb (and U/Pb) analyses are quoted at the 95% confidence interval.

The zircon U–Pb isotopic results for samples 10HH-31A and 10HH-67B were analyzed with a VG PlasmaQuad Excell inductively coupled plasma-mass spectrometer (ICP-MS) equipped with a New Wave Research LUV213 laser ablation system at the University of Hong Kong. Analytical settings were a beam diameter of ca. 40 μm, a 10 Hz repetition rate, and energy of 0.6–1.3 mJ per pulse. The equipment was tuned with total U signals ranging from 3 × 104 to 100 × 104 counts, depending on U contents. Typical ablation time was 30–60 s, leading to pits of 20–40 μm deep. Helium carrier gas transported the ablated sample materials from the laser-ablation cell via a mixing chamber to the ICPMS after mixing with Ar gas. The detailed analytical procedure of Xia et al. (2004) is followed. Data reduction for all samples was carried out using the Isoplot/Ex v. 3 program (Ludwig, 2001). The U–Pb dating results and sampling locations for 10HH-31A, 10HH-67A and 10HH-67B are listed in Table 1 and shown in Fig. 2b and c.

For whole-rock elemental and isotopic analysis, the representative samples were pulverized to 200-mesh. Major element oxides were analyzed at the Guangzhou Institute of Geochemistry (GIG), CAS, by a wavelength X-ray fluorescence spectrometry

Table 2
Major element (in wt.%) and trace element (in ppm) compositions of the Neoproterozoic amphibolites along the Ailaoshan suture zone.

Sample	Group 1					Group 2						
	10HH-31A	10HH-31C	10HH-31D	10HH-31E	10HH-31F	10HH-67A	10HH-67B	10HH-67D	10HH-67F	10HH-69A	10HH-69C	10HH-69E
SiO_2	51.45	49.34	47.61	47.08	50.92	48.55	48.63	49.03	48.87	47.29	46.81	46.85
TiO_2	0.37	0.46	0.71	0.76	0.56	1.84	1.67	1.71	1.84	2.22	2.21	2.20
Al_2O_3	15.15	14.56	14.43	13.16	14.81	11.89	10.77	10.84	11.97	14.38	14.40	14.47
$Fe_2O_3^T$	7.88	8.01	8.95	9.94	8.81	12.90	12.58	12.85	13.13	14.54	14.57	14.48
MgO	8.82	11.02	11.45	12.07	9.21	10.09	11.30	11.57	9.97	6.83	7.03	6.98
CaO	12.47	12.57	12.94	13.59	11.07	10.70	10.68	9.99	10.33	11.61	12.00	11.88
K_2O	0.75	0.83	0.81	0.59	0.81	0.23	0.16	0.16	0.25	0.62	0.53	0.46
Na_2O	2.42	2.37	2.21	2.18	2.88	2.03	1.51	1.46	2.01	1.17	1.15	1.20
MnO	0.14	0.14	0.13	0.14	0.13	0.17	0.15	0.16	0.16	0.19	0.20	0.20
P_2O_5	0.04	0.03	0.06	0.02	0.04	0.24	0.21	0.21	0.24	0.29	0.28	0.29
L.O.I	0.43	0.61	0.58	0.41	0.58	1.21	2.16	1.87	1.11	0.70	0.66	0.85
Total	99.93	99.94	99.88	99.94	99.82	99.86	99.83	99.85	99.89	99.85	99.85	99.85
mg-number	72	76	75	74	71	65	68	68	64	52	53	53
Sc	36.9	35.2	37.9	39.5	363.4	41.2	43.9	43.2	40.5	35.2	37.9	36.6
V	147	160	136	173	141	311	301	300	304	326	354	337
Cr	220	220	501	649	301	438	561	556	417	103	108	104
Co	32.7	35.1	31.1	38.6	30.8	56.4	57.4	57.3	53.2	50.2	52.5	48.5
Ni	9.7	15.4	18.7	21.5	11.9	119.3	127.0	130.4	116.7	100.3	105.3	99.9
Ga	14.2	14.9	15.2	15.9	13.5	16.3	14.9	14.9	16.2	17.7	18.2	18.4
Rb	10.6	12.6	15.9	21.1	8.5	5.1	2.0	2.1	6.0	11.8	19.7	12.7
Sr	432	399	373	308	406	458	303	298	487	238	278	242
Y	19.2	19.7	19.8	19.9	19.0	21.6	20.3	19.4	22.5	23.0	24.8	23.6
Zr	48.3	49.2	52.7	57.9	45.1	142.0	131.4	129.8	148.2	140.6	145.8	141.1
Nb	4.07	3.26	4.32	5.22	3.19	16.19	14.37	14.28	16.00	16.61	17.64	18.43
Cs	0.65	0.70	0.71	0.76	0.57	0.27	0.07	0.06	0.34	1.18	1.64	0.98
Ba	139.2	141.5	159.3	194.2	110.5	76.9	31.1	30.5	137.2	138.6	217.0	129.7
La	12.67	14.35	14.05	14.82	11.98	20.19	18.22	18.62	21.00	20.96	22.56	21.89
Ce	28.23	28.34	28.94	28.49	25.22	46.27	41.36	41.75	47.04	49.28	50.77	48.84
Pr	3.89	4.01	4.16	4.21	3.52	6.30	5.62	5.70	6.24	7.02	6.87	6.55
Nd	16.75	18.46	19.28	20.19	14.21	27.17	24.12	24.56	27.72	26.89	28.72	27.38
Sm	3.70	3.98	4.10	4.12	3.61	5.58	5.11	5.09	5.67	5.46	5.97	5.61
Eu	0.87	0.80	0.78	0.72	0.83	1.76	1.64	1.58	1.79	1.81	1.91	1.79
Gd	3.45	3.43	3.42	3.50	3.44	5.14	4.80	4.92	5.37	5.27	5.73	5.39
Tb	0.60	0.52	0.59	0.60	0.56	0.84	0.78	0.77	0.87	0.86	0.92	0.88
Dy	3.41	3.43	3.47	3.52	3.40	4.34	4.18	4.16	4.48	4.95	5.05	4.84
Ho	0.69	0.70	0.71	0.71	0.69	0.86	0.83	0.81	0.89	1.11	1.01	0.98
Er	1.80	1.79	1.80	1.82	1.78	2.15	2.06	2.04	2.18	2.57	2.55	2.48
Tm	0.26	0.26	0.27	0.28	0.23	0.30	0.30	0.28	0.31	0.38	0.37	0.37
Yb	1.76	1.76	1.77	1.80	1.73	1.94	1.81	1.82	2.00	2.30	2.32	2.29
Lu	0.28	0.28	0.26	0.28	0.27	0.29	0.27	0.27	0.30	0.33	0.36	0.34
Hf	1.27	1.51	1.70	1.80	1.39	3.88	3.57	3.50	3.95	3.87	3.91	3.65
Ta	0.31	0.32	0.34	0.39	0.29	1.11	1.01	1.00	1.16	1.20	1.27	1.21
Pb	9.83	9.93	11.00	11.59	8.45	5.15	3.71	4.37	5.16	13.37	13.46	13.23
Th	1.26	1.38	1.50	1.63	1.14	2.36	2.12	2.03	2.46	2.90	3.06	2.93
U	1.06	1.23	1.29	1.54	0.81	0.55	0.49	0.45	0.56	0.65	0.64	0.65
$\sum$REE	78.36	82.11	83.59	85.05	71.47	123.13	111.09	112.37	125.87	129.20	135.10	129.61

Table 3
Sr–Nd isotopic compositions of the amphibolites along the Ailaoshan suture zone.

Sample	Sm	Nd	Rb	Sr	$^{147}Sm/^{144}Nd$	$^{143}Nd/^{144}Nd$	2σ	$(^{143}Nd/^{144}Nd)_i$	$^{87}Rb/^{86}Sr$	$^{87}Sr/^{86}Sr$	2σ	$(^{87}Sr/^{86}Sr)_i$	ε_{Nd}
Group 1													
10HH-31A	3.70	16.75	10.64	432.40	0.1334	0.512129	13	0.511429	0.0712	0.707009	11	0.706196	−3.45
10HH-31C	3.98	18.46	12.68	498.50	0.1304	0.512186	13	0.511502	0.0736	0.706758	13	0.705917	−2.04
10HH-31D	4.10	19.28	15.92	532.70	0.1284	0.512109	11	0.511435	0.0865	0.705917	13	0.704929	−3.34
10HH-31F	3.61	14.21	8.49	405.60	0.1537	0.512263	10	0.511457	0.0606	0.707319	12	0.706627	−2.91
Group 2													
10HH-67A	5.58	27.17	5.11	457.70	0.1242	0.512476	8	0.511814	0.0323	0.706913	13	0.706537	4.39
10HH-67D	5.09	24.56	2.12	297.50	0.1253	0.512476	6	0.511808	0.0206	0.707234	13	0.706995	4.28
10HH-69A	5.46	26.89	11.85	238.40	0.1228	0.512461	8	0.511806	0.1438	0.709238	12	0.707568	4.24
10HH-69E	5.61	27.38	12.73	242.40	0.1238	0.512457	8	0.511795	0.1520	0.712167	12	0.710398	4.08

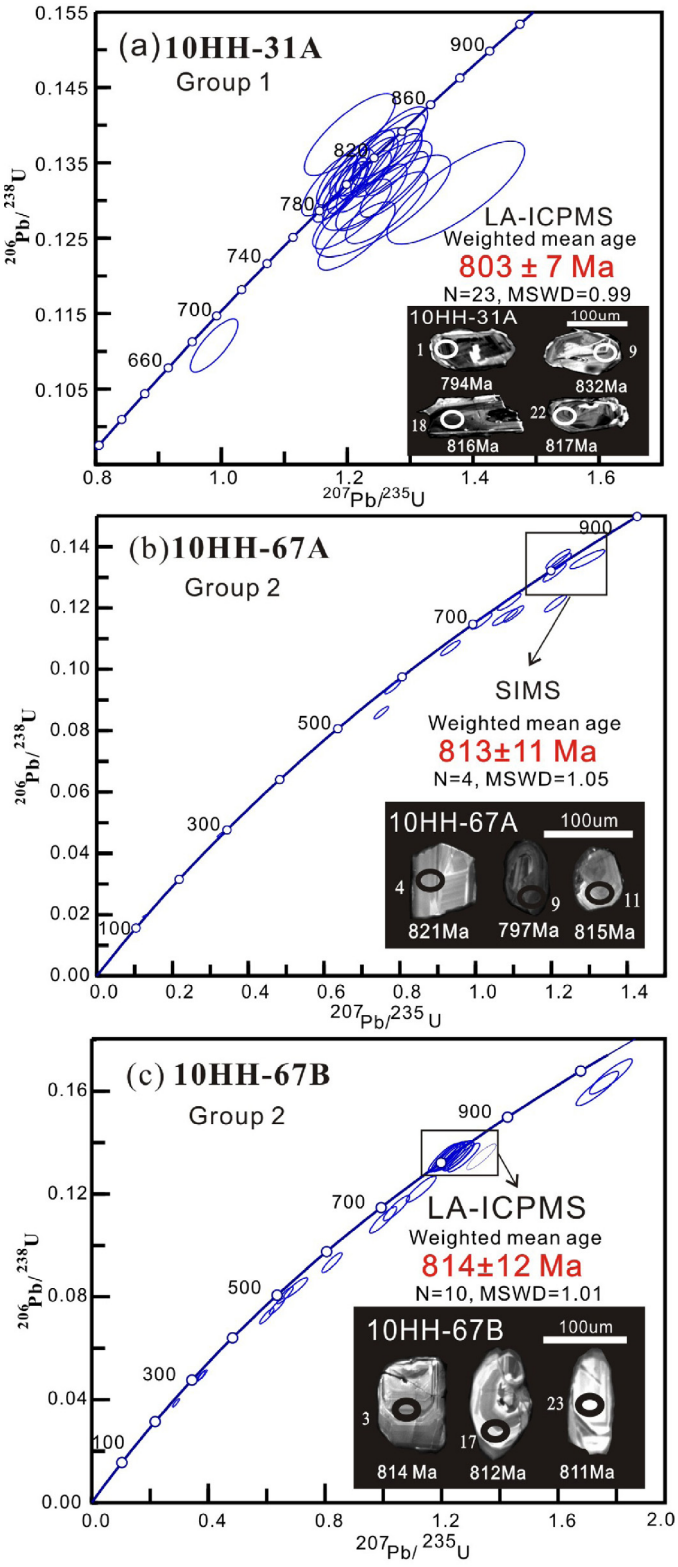

Fig. 4. Zircon U–Pb concordia diagram for amphibolites along the Ailaoshan suture zone. (a) 10HH-31A amphibolite at Qingjiao (Jinping), (b) 10HH-67A amphibolite at Yiwanshui (Yuanyang), and (c) 10HH-67B amphibolite at Yiwanshui (Yuanyang).

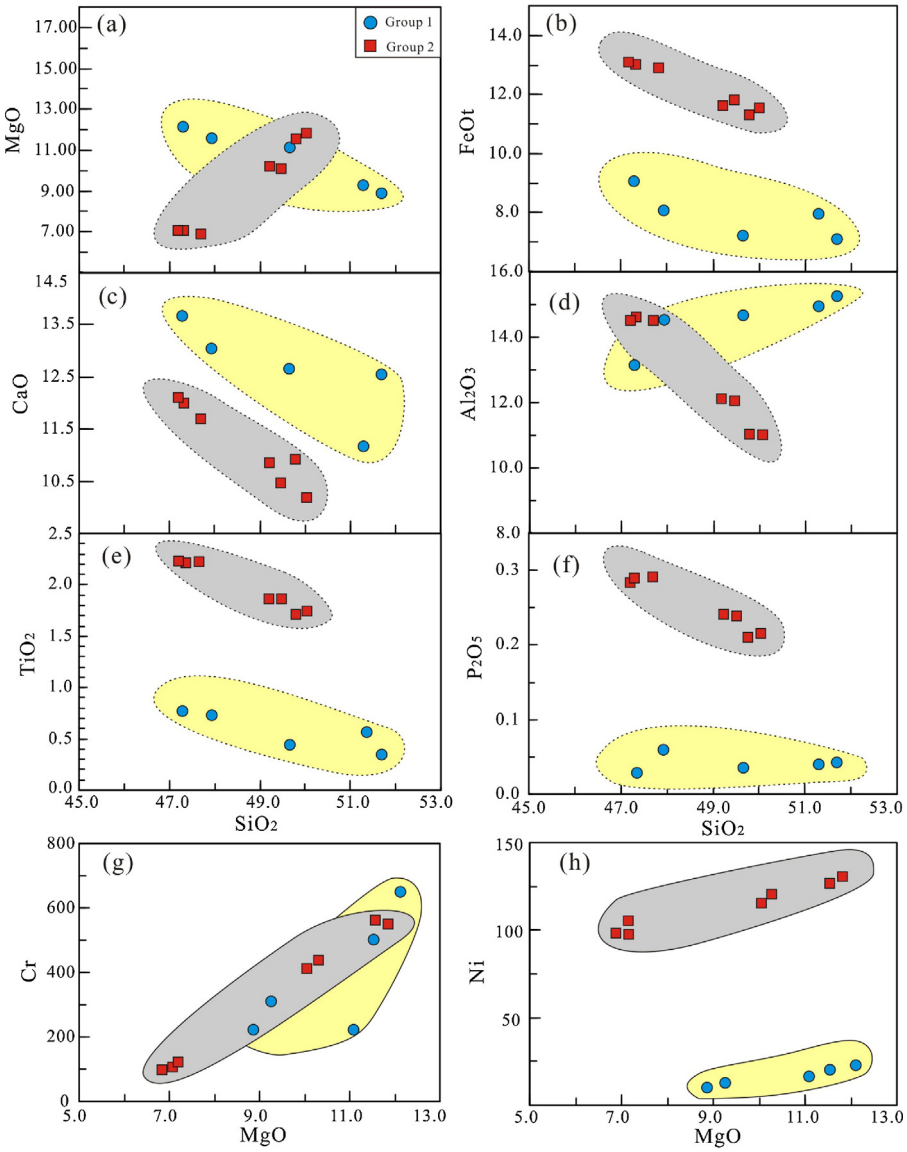

Fig. 5. Plots of SiO_2 versus (a) MgO, (b) FeOt, (c) CaO, (d) Al_2O_3, (e) TiO_2, (f) P_2O_5, and MgO versus (g) Cr and (h) Ni for amphibolites from the Ailaoshan suture zone.

using a Rigaku ZSX100e spectrometer with the relative standard derivations of <5%. Trace element contents were measured using Perkin-Elmer Sciex ELAN 6000 ICP-MS at the GIG, CAS. Detailed sample preparation and analytical procedure of Qi et al. (2000) is followed. Sample powders for Sr and Nd isotopic analyses were spiked with mixed isotope tracers, dissolved in Teflon capsules with HF+HNO_3 acids, and separated by conventional cation-exchange technique and run on single W and Ta-Re double filaments. Sr–Nd isotope ratios were measured on a Micro-Mass Isoprobe MC-ICP-MS at the GIG, CAS. Sample preparation and chemical separation followed Liang et al. (2003). The total procedure blanks for Sr were 200–500 pg and <50 pg for Nd. $^{86}Sr/^{88}Sr = 0.1194$ and $^{146}Nd/^{144}Nd = 0.7219$ were used for correcting the mass fractionation for Sr and Nd isotopic ratios, respectively. The measured $^{87}Sr/^{86}Sr$ ratio of the (NIST) SRM 987 standard and $^{143}Nd/^{144}Nd$ ratio of the La Jolla standard is 0.710265 ± 12 (2σ) and 0.511862 ± 10 (2σ), respectively. Within-run errors of precision are estimated to be better than 0.000015 for $^{86}Sr/^{88}Sr$ and $^{146}Nd/^{144}Nd$ in the 95% confidence level during the analytical process. The analytical results of major oxides, elements and Sr–Nd isotopes are shown in Tables 2 and 3.

4. Results

4.1. Zircon U–Pb geochronology

Zircons from samples 10HH-31A, 10HH-67A and 10HH-67B are generally transparent to translucent, light-brown to colorless grains or grain fragments with subhedral morphology. They are ~80–120 μm in length with length to width ratios of 1.5:1 to 3:1. CL images exhibit weak oscillatory zoning with variable luminescence, indicative of an igneous origin (Fig. 4a–c).

4.1.1. 10HH-31A

Zircon grains have U contents ranging from 117 ppm to 1138 ppm and Th from 136 to 571 ppm. Their Th/U ratios are in range of 0.49–1.78 (Table 1). Twenty-four analyses on 23 grains form a coherent cluster and give a $^{206}Pb/^{238}U$ weighted mean age of 803 ± 7 Ma with MSWD = 0.99 (Fig. 4a). In combination with the oscillatory zoning of the grains, this age can be interpreted as the formation age of the sample.

4.1.2. 10HH-67A

The U and Th concentrations for the sixteen analyzed grains range from 139 to 1288 ppm and 48 to 3400 ppm, respectively, with Th/U ratios of 0.28–1.03 (Table 1). Most of the analyses are variably discordant, interpreted to be the result of late Pb loss. Four spots yield a coherent group with the $^{206}Pb/^{238}U$ weighted mean age of 813 ± 11 Ma with MSWD = 1.05 (Fig. 4b), representing the crystallization age of the sample.

4.1.3. 10HH-67B

Twenty-six analyses on 26 grains exhibit a relatively wide range of U and Th concentrations with U = 112–1608 ppm and Th = 55–542 ppm. Th/U ratios range from 0.10 to 1.20 (Table 1). The majority of the 26 analyses form a normally discordant array with the apparent $^{207}Pb/^{206}Pb > ^{207}Pb/^{235}U > ^{206}Pb/^{238}U$, suggestive of Pb loss during subsequent tectonothermal events. Four grains have significantly older U–Pb ages than the remaining analyses with the $^{207}Pb/^{206}Pb$ apparent ages of 2740 Ma, 2087 Ma, 1146 Ma and 1150 Ma (Table 1), and are interpreted as xenocrysts. Ten spots yield a $^{206}Pb/^{238}U$ weighted mean age of 814 ± 12 Ma with MSWD = 1.01 (Fig. 4c), representing the formation age of the sample.

4.2. Geochemical characteristics

Based on the mineral assemblage and geochemical characteristics, the amphibolites from Jinping and Yuanyang are divided into two groups, referred to as Group 1 and Group 2. Group 2 samples have higher FeOt, TiO_2 and P_2O_5 contents and lower CaO contents than Group 1 (Table 2 and Fig. 5). Ni contents of Group 2 are relatively higher (100–130 ppm) compared to the values of 10–22 ppm for Group 1. On the plot of Zr/TiO_2 versus Nb/Y, Group 1 falls in the subalkaline field, whereas Group 2 samples plot in the alkaline field (Table 2 and Fig. 6a). Group 1 has mg-number of 71–76, La/Yb of 7.2–7.7, TiO_2 of 0.37–0.76 wt.% and Nb of 3.19–5.22 ppm (Figs. 6b and 7). Group 2 samples, are characterized by mg-number of 52–68 and La/Yb of 9.1–10.5 (Fig. 6b) with TiO_2 contents ranging from 1.67 wt.% to 2.22 wt.% and Nb contents from 14.28 ppm to 18.43 ppm.

On REE-normalized plot, Group 1 has (La/Yb)cn of 4.98–5.91 and (Gd/Yb)cn of 1.60–1.65, and negative europium anomalies with δEu (2*Eu/(Sm + Gd)) of 0.58–0.74 (Fig. 7a). Group 2 has a steeper REE-normalized pattern with higher LREEs contents, (La/Yb)cn (6.55–7.52), (Gd/Yb)cn (1.90–2.23) and δEu (0.97–1.01) ratios than Group 1 (Fig. 7c). On multi-element primitive mantle-normalized plot, Group 1 samples are characterized by negative Nb–Ta ((Nb/La)n = 0.22–0.34) and P–Ti anomalies and positive Sr anomalies. Group 2 has (Nb/La)n ratios ranging from 0.73 to 0.81, (Th/La)n ratios from 0.88 to 1.12 and (Hf/Sm)n from 0.93 to 1.02, and is marked by enrichment in LILEs and weak depletion in Nb–Ta and Ti (Fig. 7b and d).

The initial Sr–Nd isotopic compositions for groups 1 and 2 are calculated back to their formation age of ~800 Ma and ~810 Ma, respectively (Fig. 8b and Table 3). $^{87}Sr/^{86}Sr(t)$ ratios for Group 1 range from 0.70493 to 0.70663 and have $\varepsilon_{Nd}(t)$ values of −3.45 to −2.04. In contrast, Group 2 display distinct Sr–Nd isotopic compositions with $^{87}Sr/^{86}Sr(t)$ ratios ranging from 0.71040 to 0.70654 and $\varepsilon_{Nd}(t)$ values from +4.08 to +4.39.

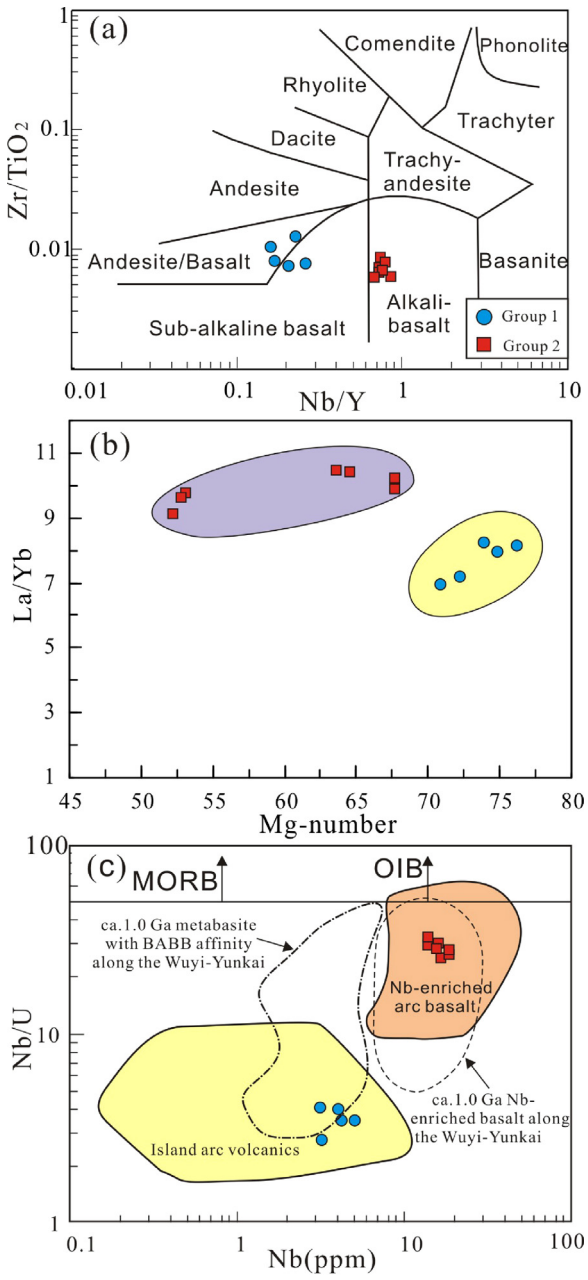

Fig. 6. Classification plots of (a) Zr/TiO_2 versus Nb/Y (Winchester and Floyd, 1977), (b) La/Yb versus mg-number and, (c) Nb/U versus Nb (Kepezhinskas et al., 1996) for the amphibolites along the Ailaoshan zone. The fields of the island arc basalts and Nb-enrich basalt are from (Kepezhinskas et al., 1996). The data for ~1.0 Ga metabasite with the affinity to back-arc-basin basalt and Nb-enriched arc basalt from the Cathaysia Block are from Wang et al. (2013b). Symbols in (b–c) are the same as those in (a).

5. Discussion

5.1. Alteration effects

Groups 1 and 2 samples have experienced greenschist to amphibolite facies metamorphism. They show low loss on ignition (LOI) of less than 2.2 wt.%. High field strength elements (e.g., Th, Zr, Hf, Nb, Ta, Ti, Y and REE) and Nd isotopic compositions are generally considered to be immobile during alteration or weathering (e.g., Barnes et al., 1985; Wang et al., 2007a) and Zr is often used as a reference phase to test the mobility of other incompatible elements (Rolland et al., 2009). Our samples show positive correlation between Zr and Nb, Th, La, Yb, Nd, Sm and Ti for groups 1 and 2, whereas LOI shows little or no correlation with Nb/La and Th/La ratios and $\varepsilon_{Nd}(t)$ values (not shown). These signatures, together with the subparallel REE and multi-element patterns in Fig. 7a–d, suggest that the behavior of these elements can be used to trace the primary magmatic features. Furthermore, the linear correlations

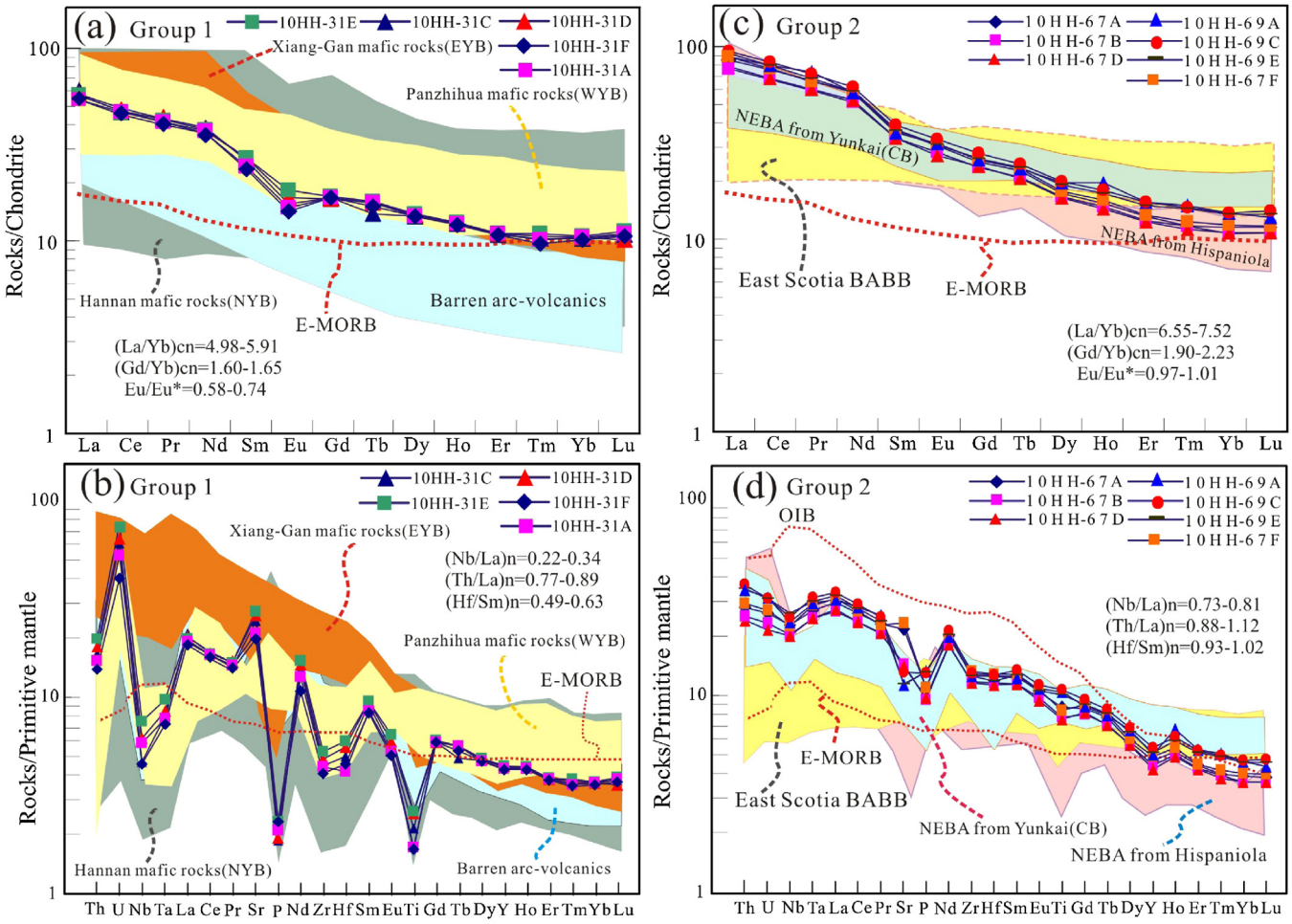

Fig. 7. Chondrite-normalized REE patterns and primitive mantle-normalized incompatible element spidergrams for the amphibolites along the Ailaoshan suture zone. Abbreviations: SYB, Southern Yangtze Block; WYB, Western Yangtze Block; NYB, Northern Yangtze Block; EYB, Eastern Yangtze Block; CB, Cathaysia Block. The normalized values for the chondrite and primitive mantle are from Sun and McDonough (1989). Data for the Barren arc-volcanic rocks and East Scotia back-arc-basin are from Luhr and Haldar (2006) and Leat et al. (2000), respectively. OIB, N-MORB and E-MORB are after Sun and McDonough (1989). Nb-enriched basaltic andesite from Hispaniola and Yunkai are from Viruete et al. (2007) and Zhang et al. (2012a), respectively. Panzhihua mafic rocks are from Zhao and Zhou (2007) and Li et al. (2006) and references therein. Hannan mafic rocks are from Zhao and Zhou (2009), Dong et al. (2011), Ling et al. (2003). Xiang-Gan mafic rocks are from Wang et al. (2008b), Li et al. (2008b) and references therein.

on the Harker variation diagrams (Fig. 5) also display insignificant effects of alteration.

5.2. Petrogenesis of the Ailaoshan amphibolite

The positive correlation between Al_2O_3 and SiO_2 but negative correlation between CaO and SiO_2 of the Group 1 samples suggest a source characterized by low Al_2O_3 and high CaO (Upton and Emeleus, 1987). Such signatures, combined with MgO of 8.82–12.07 wt.%, P_2O_5/Al_2O_3 of 0.002–0.004 and Gd/Yb of 1.9–2.0 (Table 2), are most likely inherited from a garnet-bearing, orthopyroxene-rich source that had previously experienced melt extraction (e.g., Hirose, 1997; Wang et al., 2007c, 2013a). Group 1 samples show enrichment in LILEs and depletion in HFSEs with pronounced negative Nb–Ta and Zr–Hf anomalies (Fig. 7b). These signatures, together with high Th/Yb (0.66–0.90), Ba/Nb, Zr/Nb, Sr/La and Th/Ce ratios and low Nb/La, Ta/La and Ce/Pb ratios, indicate the similarity to typical supra-subduction zone arc magmatic rocks and distinction from rocks in intraplate settings (Fig. 9c, e.g., Pearce, 2008; Luhr and Haldar, 2006; Pearce and Peate, 1995). The REE-normalized and multi-element primitive mantle normalized patterns of Group 1 are also identical to the Barren Arc volcanic rocks and Neoproterozoic Panzhihua mafic rocks (Fig. 7a and c).

Group 1 samples have negative $\varepsilon_{Nd}(t)$ values of −2.04 to −3.45 (Table 3 and Fig. 8b), indicate the involvement of crustal components rather than the addition of new slab-derived fluid/melt within the magma source region (e.g., Wang et al., 2004, 2007c, 2013b). Possible sources for crustal involvement include arc basement or the subduction-derived sediments. Our modeling calculation suggests that ~10–30% SCC crustal materials are required to achieve the observed Nd isotopic composition of the Group 1 samples (Fig. 8a–d, e.g., Chen and Jahn, 1998; Wang et al., 2007c, 2011, 2012b). Such a large volume of crustal materials in the mantle source is inconsistent with the Sr–Nd isotopic compositions and the ratios of incompatible elements, and also fails to explain the major oxide characteristics of the Group 1 samples. As a result, an alternative model for the petrogenesis of the Group 1 samples is proposed involving recent or ancient metasomatism of subduction-derived sedimentary components. Such a petrogenesis can reasonably explain the geochemical signature of the Group 1 samples, such as the correlations between Nb/Y, Rb/Y, Nb/Zr, Th/Zr, Nb/U, Th/Nb, Ba/Nb and $\varepsilon_{Nd}(t)$ (Fig. 11a, c and d; e.g., Fan et al., 2010; Kepezhinskas et al., 1997; Pearce and Stern, 2006; Zhao and Zhou, 2007).

Group 2 shows lower Al_2O_3, K_2O and CaO and higher P_2O_5/Al_2O_3 (0.019–0.020), Nb/Ta (13.8–15.2), Ce/Y (2.04–2.15), Sm/Yb (2.4–2.9) and Gd/Yb (2.3–2.7) in comparison with Group 1

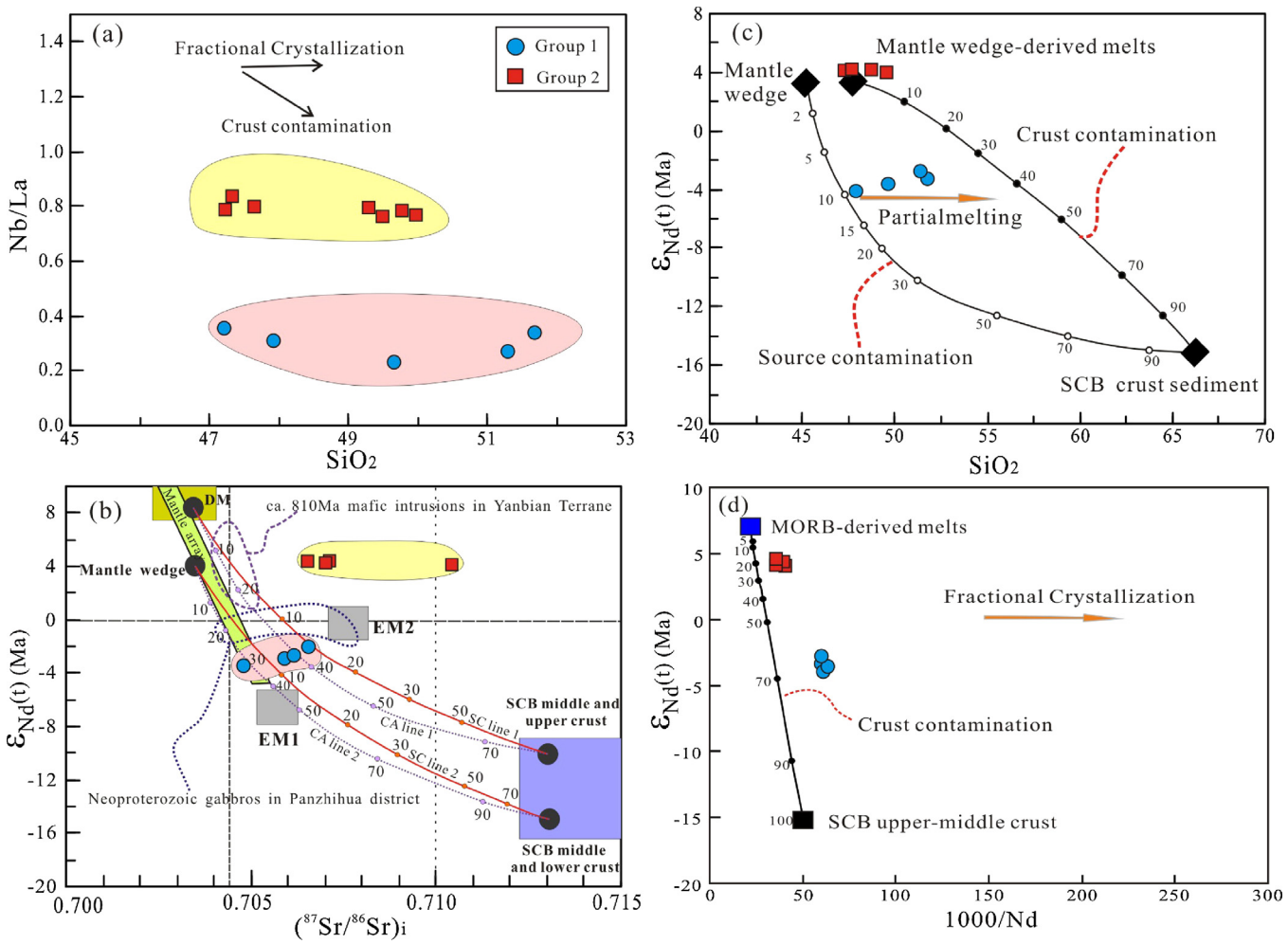

Fig. 8. Plots of (a) Nb/La versus SiO_2, (b) $\varepsilon_{Nd}(t)$ versus $(^{87}Sr/^{86}Sr)_i$ (c) SiO_2 versus $\varepsilon_{Nd}(t)$ (Wang et al., 2013a) and (d) 1000/Nd versus $\varepsilon_{Nd}(t)$ (Zhang et al., 2012a). Data for the Neoproterozoic (~810 Ma) mafic intrusions in Yanbian Terrane and Neoproterozoic gabbros in Panzhihua of the western Yangtze Block are from Zhou et al. (2006b) and Zhao and Zhou (2007). SC lines 1 and 2 (red solid line) note source contamination of the depleted mantle and wedge with SCC crustal sediment, respectively. SC line 2 denotes the delamination of the SCB basement into the lithospheric mantle. CA lines 1 and 2 (pale blue dashed line) mean crustal assimilation en route for the depleted mantle- and wedge-derived magma with SCB crust, respectively. The modeling results show that the ~10–30% average crustal materials are required to be involved in the MORB-derived magma by crustal contamination en route for matching the observed Nd isotopic compositions but failing to interpret the variation of Nb/La ratios for groups 1 and 2. (For interpretation of the references to color in this figure legend, the reader is referred to the web version of this article.)

(Table 2 and Fig. 5a–h). These features indicate a derivation from a mantle source more enriched in garnet and which has undergone little or no depletion by a previous melt extraction event (e.g., Class et al., 2000). The Nb/U values for Group 2 are markedly lower than those of the average ocean island basalts (Fig. 6c). On the Gd/Yb versus Nb/La discrimination diagram (Fig. 9a), Group 2 samples have higher Nb contents than typical arc volcanic rocks, and can be classified as Nb-enriched basalt (e.g., Sajona et al., 1993, 1996). Their compositions are similar to the Mindamao (Philippines) Nb-enriched island arc basalts and the early Neoproterozoic Wuyi–Yunkai Nb-enriched arc basalt from the SCC (e.g., Wang et al., 2013a; Zhang et al., 2012a). Three petrogenetic models have been proposed for Nb-enriched basalt involving (i) an OIB-like plume-related source, (ii) shallow-level crustal assimilation en route, and (iii) a mantle wedge metasomatised by young slab-derived components (e.g., Sajona et al., 1996; Kepezhinskas et al., 1996; Stern, 2002; Wang et al., 2013a). Neoproterozoic OIB-derived mafic rocks have not been observed in the study area and the geochemical characteristics of the Group 2 samples are distinct from those of OIB, ruling out a plume-related origin. Group 2 has higher FeOt, TiO_2 and P_2O_5 contents and lower CaO contents and is marked by enrichment in LILEs and insignificant in Nb–Ta and Ti (Fig. 7b and d), precluding the possibility of the significant shallow-level crustal assimilation. These samples show higher La/Yb, Th/Ce and Th/Nb ratios than average MORB (Sun and McDonough, 1989). Their Nb/Ta ratios range from 13.8 to 15.2, (Ta/La)n ratios from 0.90 to 0.96, and (Hf/Sm)n from 0.93 to 1.02. These signatures argue for the involvement of slab-derived melts in the Group 2 source. This is similar to those of Mindamao and Wuyi–Yunkai Nb-enriched basalts that are interpreted as the product of interaction of subarc mantle peridotite with siliceous slab-derived melt (Fig. 11b; e.g., Kepezhinskas et al., 1996, 1997; Wang et al., 2013a). The modification of a subduction-component in the Group 2 source is further evidenced by the correlations between Nb/Zr, Th/Zr, Nb/U, Th/Nb, Ba/Nb and ε_{Nd} (Fig. 11a–d). Group 1 has arc-like signatures, and plots above the MORB array in Fig. 9b (Pearce and Stern, 2006), similar to those of arc magma along the western and northern margins of the Yangtze Block. The majority of the Group 2 samples plot between MORB and western Yangtze arc magma, suggestive of the capture of subduction components within the magma source, identical to the Scotia back-arc basin basalt (BABB) whose source was modified by the South Sandwich arc (Fig. 9b; Pearce and Stern, 2006).

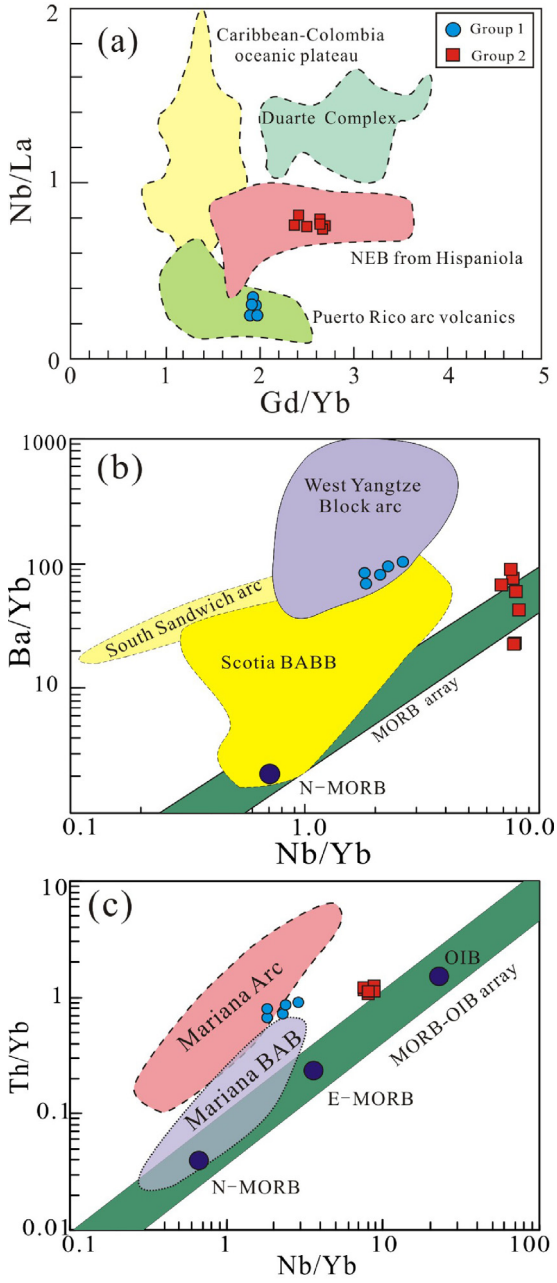

Fig. 9. Discrimination diagrams of (a) Gd/Yb versus Nb/La (Zhang et al., 2012a), (b) Ba/Yb versus Nb/Yb (Pearce and Stern, 2006), and (c) Th/Yb versus Nb/Yb (Pearce, 2008) for the amphibolites along the Ailaoshan suture zone. Back-arc basalts modified by subduction components always plot between the MORB array and arc field and those of unaffected by subduction components mostly within the MORB array. Data for the arc rocks in the west Yangtze Block (~810 Ma), South Sandwich arc-Scotia BABB and Mariana arc and BAB are from Zhou et al. (2006b), Pearce and Stern (2006) and Pearce (2008), respectively.

5.3. Tectonic implications: ~815–800 Ma arc system along the SW Yangtze Block

Our age data for amphibolites along the Ailaoshan zone give zircon U–Pb ages of 803 ± 7 Ma (Group 1), 813 ± 11 Ma (Group 2) and 814 ± 12 Ma (Group 2). Recent data for orthogneiss within the Ailaoshan zone having U–Pb zircons ages ranging from 843 Ma to 803 Ma (e.g., Li, 2010; Liu et al., 2008a). These geochronological data indicate the presence for the Neoproterozoic igneous rocks adjacent to the SW margin of the Yangtze Block. Group 1 amphibolites display an affinity to arc volcanic rocks (Figs. 6c, 9a–c and 10a). Group 2 samples show higher HFSEs and Nb contents and lower Ti/Zr, V/Ti and Sc/Y ratios than Group 1. On the plots of V versus Ti/1000, FeO*/MgO versus TiO_2 and Ti/Zr versus V/Ti (e.g., Woodhead et al., 1993; Fan et al., 2004), Group 2 samples generally plot in the field of BABB, similar to the East Scotia, North Fiji, Lau basin, Havre Trough and East Woodlark lavas (e.g., Hollings and Kerrich, 2004; Macdonald et al., 2000). Intra-oceanic BABB (e.g., South Sandwich Islands and Tonga–Kermadec arcs) is geochemically indistinguishable from an N-MORB source (e.g., Hawkins, 1995) and has (La/Yb)n < 2, Nb/La < 0.6 and Sm/Nd > 0.3. In contrast, the BABB with continental basement usually exhibits E-MORB-like elemental and isotopic compositions with (La/Yb)n > 3, Nb/La > 0.6 and Sm/Nd < 0.3 (e.g., Shinjo et al., 1999). Group 2 has elevated LILEs, LREEs and HFSEs, and relatively low (Th/La)n. Their (La/Yb)n ratios range from 6.55 to 7.52, Nb/La from 0.76 to 0.84, Sm/Nd from 0.20 to 0.21, and Zr/Y from 5.87 to 6.69, similar to those observed in Northern Okinawa Trough (Japan Sea) intra-continental BABB (e.g., Gribble et al., 1998; Sandeman et al., 2006). In plots of Ce versus Yb and Ce/Nb versus Th/Nb (Fig. 10b–d; Hawkesworth et al., 1993; Pearce, 1983), Group 2 samples plot near the field of the Okinawa BABB and resemble continental margin arc basalts from Philippines. The presence of the inherited zircons in 10HH-67A (e.g., 10HH-67A-02, -10, -19 and -24) also points to the involvement of continental basement. As a result, it is herein proposed that Group 1 samples formed in a magmatic arc environment and Group 2 in an intra-continental BAB setting. Lu (1989) also suggested, on the basis of the voluminous volcano-sedimentary associations and relatively uniform volcanic sequences in the Ailaoshan Group/Complex, the development of a Neoproterozoic arc-back-arc setting along the Ailaoshan zone.

The Neoproterozoic successions are fault-bounded both with respect to each other and with respect to the bounding Yangtze and Indochina blocks. Comparison of the geochronological and geochemical data from the Ailaoshan zone with those in the bounding blocks favors the correlation with the western margin of the Yangtze Block. The temporal equivalence of the two groups of amphibolite suggests that they originally formed in spatial proximity as part of an overall coherent supra-subduction zone tectonic assemblage. Furthermore, Neoproterozoic units have recently been recognized within the Ailaoshan suture to the southwest of the study area (Figs. 1 and 12), with gabbro and granodiorite yielding U–Pb zircon ages of 769 ± 7 Ma and 761 ± 11 Ma and their geochemical composition suggesting a magmatic arc setting (e.g., Qi et al., 2012). Additionally, in the PoSen complex in northern Vietnam, which is inferred to lie along a further extension of the Ailaoshan suture zone (Hieu et al., 2009, 2012), the granitic rocks were dated at 760–751 Ma and show subduction-related geochemical signatures (Figs. 1 and 12 and Supplementary Table 1; e.g., Hieu et al., 2009, 2012; Lin et al., 2012; Liu et al., 2012; Wang et al., 2011a). The synthesis of all data suggests an overall age-range of the Neoproterozoic igneous activity within the Ailaoshan suture zone from at least 815 Ma to 750 Ma. This falls within the overall age-range (860–730 Ma) of supra-subduction activity along the western margin of the Yangtze Block (e.g., Zhao and Cawood, 2012; Zhao et al., 2011; Zhao and Zhou, 2007; Zhou et al., 2002a,b, 2006a,b). This contrasts with the time (~1000–820 Ma) of the subduction-related magmatic activity along the Wuyi–Yunkai, Shuangxiwu and Jiangnan Orogens in the eastern and central parts of the SCC (Fig. 1; e.g., Cawood et al., 2013; Shu et al., 2008, 2011; Wang et al., 2013b; Zhang et al., 2012a,b, 2013b). If the Neoproterozoic igneous rocks within the Ailaoshan suture zone represent the disrupted southward extension of the subduction-related rocks along the western margin of the Yangtze Block, then their current disposition requires at least 400 km of left-lateral strike slip displacement along the suture and the younger Cenozoic faults (e.g., Leloup et al., 1995; Tapponnier et al., 1990).

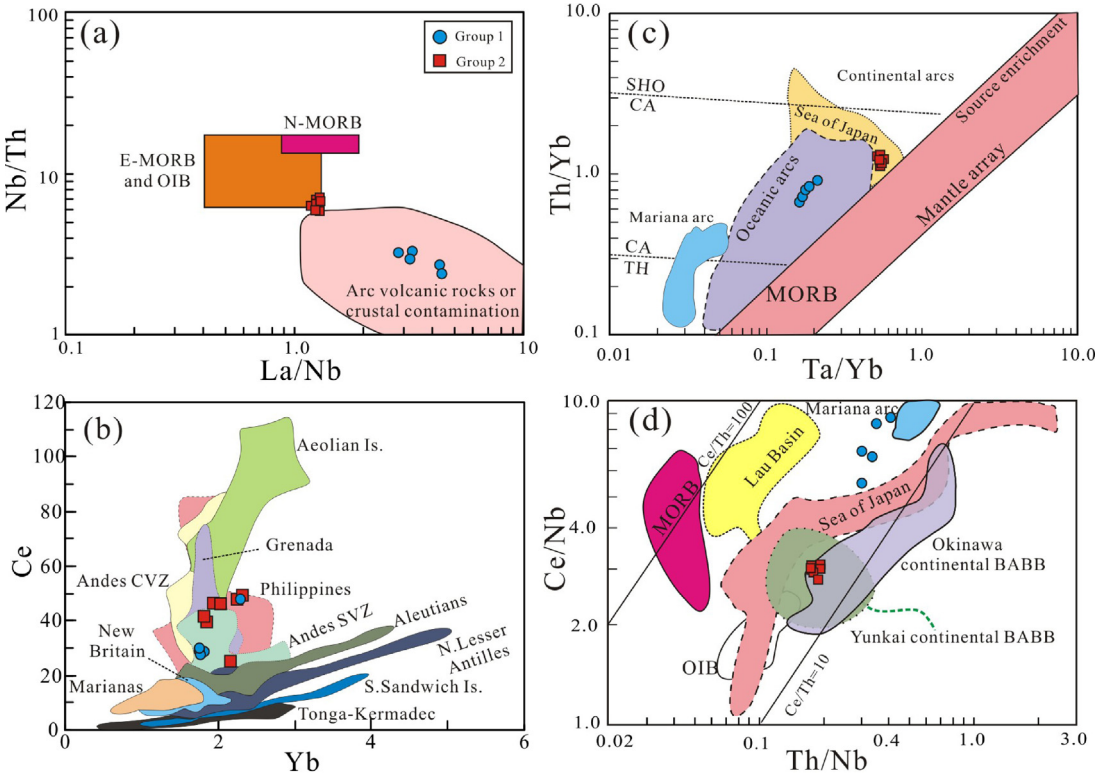

Fig. 10. (a) Nb/Th versus La/Nb. (b) Ce versus Yb (Hollings and Kerrich, 2004), (c) Ta/Yb versus Th/Yb (Pearce and Peate, 1995), and (d) Th/Nb versus Ce/Nb (Zhang et al., 2012a) for the amphibolites along the Ailaoshan zone.

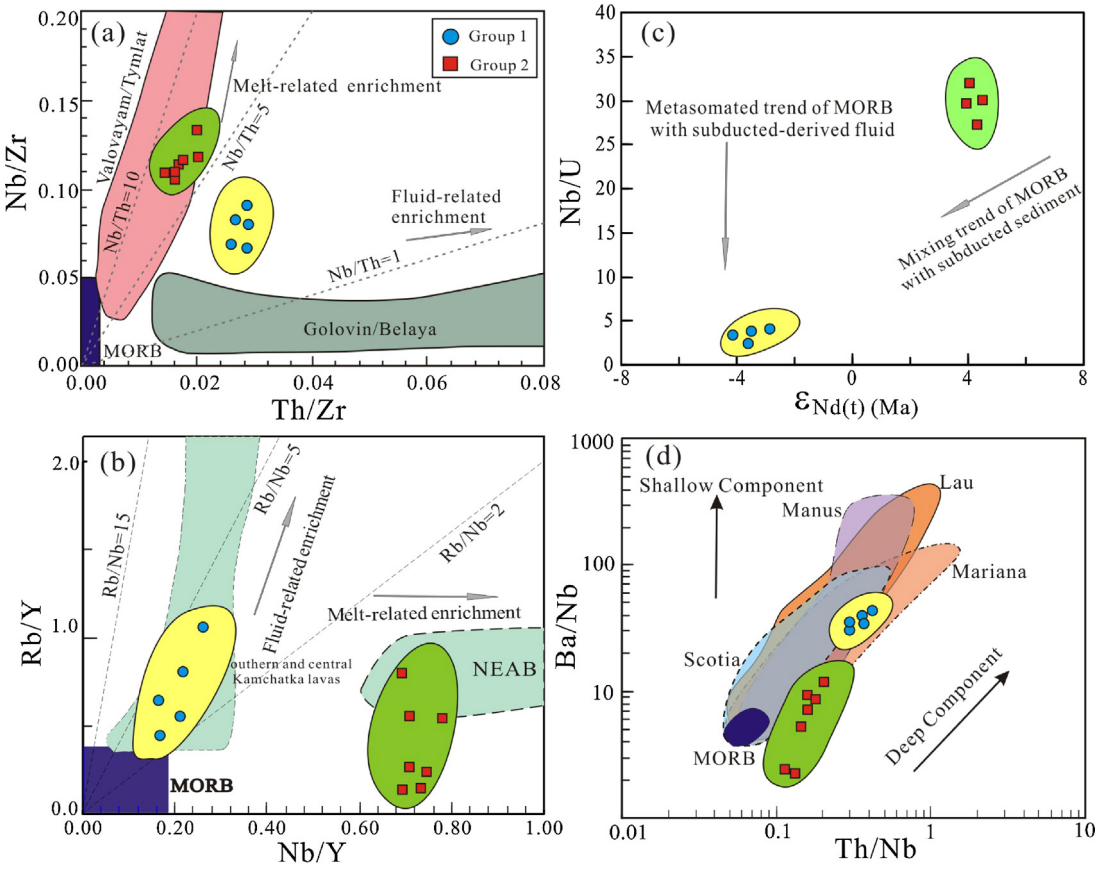

Fig. 11. Discrimination diagrams of (a) Nb/Zr versus Th/Zr (Zhao and Zhou, 2007), (b) Nb/Y versus Rb/Y (Kepezhinskas et al., 1997), (c) Nb/U versus $\varepsilon_{Nd}(t)$ (Fan et al., 2010), and (d) Th/Nb versus Ba/Nb (Pearce and Stern, 2006) for the amphibolites along the Ailaoshan zone.

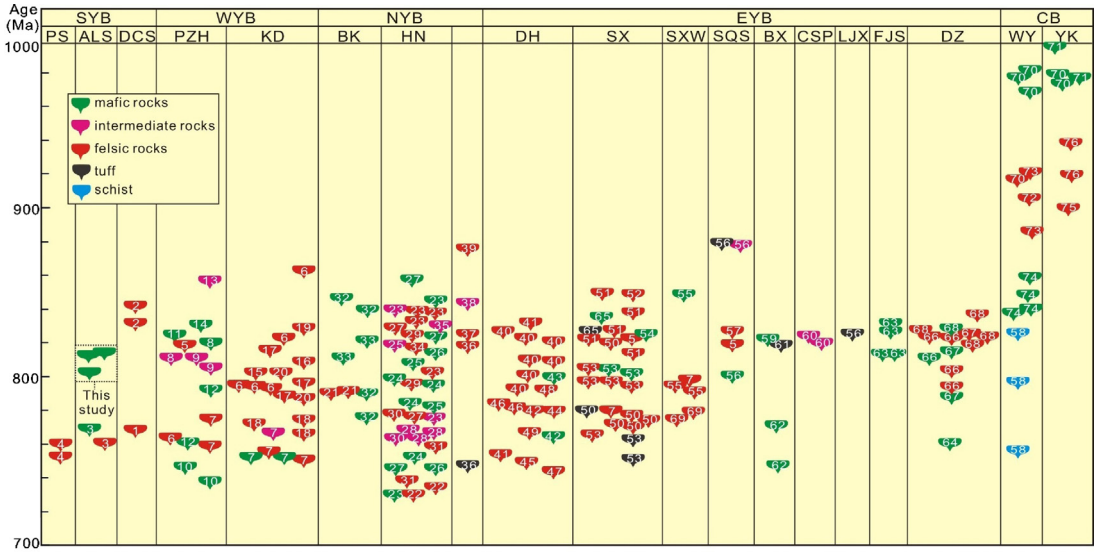

Fig. 12. Age range of principal Neoproterozoic rocks around the Yangtze Block. Abbreviations: SYB, Southern Yangtze Block; WYB, Western Yangtze Block; NYB, Northern Yangtze Block; EYB, Eastern Yangtze Block; CB, Cathaysia Block; PS, PoSen; ALS, Ailaoshan; DCS, Diancangshan; PZH, Panzhihua; KD, Kangding; BK, Bikou; HN, Hannan; DH, Donghai; SX, Shangxi; SXW, Shuangxiwu; SQS, Shuangqiaoshan; BX, Banxi; CSP, Cangshuipu; LJX, Lengjiaxi; FJS, Fangjingshan; DZ, Danzhou; WY, Wuyi; YK, Yunkai. Numbers on data points refer to the following sources: 1. Lin et al. (2012), 2. Liu et al. (2008a), 3. Qi et al. (2012), 4. Wang et al. (2011a), 5. Li et al. (2003b), 6. Zhou et al. (2002b), 7. Li et al. (2003a), 8. Sinclair (2001), 9. Zhou et al. (2006b), 10. Zhao and Zhou (2007), 11. Zhu et al. (2006), 12. Zhu et al. (2008), 13. Li et al. (2003c), 14. Du et al. (2007), 15. Li et al. (2002), 16. Ma et al. (1989), 17. Zhao et al. (2008), 18. Huang et al. (2008), 19. Roger and Calassou (1997), 20. Ling et al. (2001), 21. Pei et al. (2009), 22. Zhao and Zhou (2008), 23. Xia et al. (2009), 24. Dong et al. (2011), 25. Zhou et al. (2002a), 26. Zhao and Zhou (2009), 27. Dong et al. (2012), 28. Zhao et al. (2010), 29. Zhang et al. (2000), 30. Zhao et al. (2006), 31. Zhang et al. (2004), 32. Yan et al. (2004), 33. Wang et al. (2008c), 34. Ling et al. (2003), 35. Liu and Zhang (2013), 36. Ma et al. (1984), 37. Zhao et al. (2013), 38. Bao et al. (2008), 39. Zhang et al. (2006), 40. Chen et al. (2013), 41. Xu et al. (2001), 42. Xu et al. (2006), 43. Liu et al. (2008b), 44. Chen et al. (2010), 45. Liu et al. (2004), 46. Chen et al. (2007), 47. Chen et al. (2003), 48. Hacker et al. (2006), 49. Hu et al. (2007), 50. Zheng et al. (2008), 51. Xue et al. (2010), 52. Li et al. (2010), 53. Wang et al. (2012a), 54. Zhang et al. (2012c), 55. Li et al. (2008a), 56. Wang et al. (2008a), 57. Li et al. (2008b), 58. Wu et al. (2010), 59. Wang et al. (2007b), 60. Zhang et al. (2012b), 61. Zhang et al. (2013a), 62. Wang et al. (2008b), 63. Zhou et al. (2009), 64. Ge et al. (2001), 65. Yin et al. (2013), 66. Wang et al. (2006), 67. Zeng et al. (2005), 68. Li (1999), 69. Wang et al. (2010), 70. Wang et al. (2013b), 71. Zhang et al. (2012a), 72. Ye et al. (2007), 73. Li et al. (2009b), 74. Shu et al. (2011), 75. Qin et al. (2006), 76. Zhang et al. (1998).

Supplementary material related to this article can be found, in the online version, at http://dx.doi.org/10.1016/j.precamres.2014.01.009.

The arc and back-arc affinities of the Neoproterozoic igneous rocks along the Ailaoshan suture zone (Figs. 7, 9 and 10a; Qi et al., 2012; Wang et al., 2011a) are consistent with the supra-subduction setting inferred for the similar age igneous activity within the SCC (Figs. 1 and 11; Cawood et al., 2013; Wang et al., 2013b; Zhou et al., 2002a,b). Our samples show no evidence for plume or within-plate geochemical affinities, further suggesting that the convergent plate margin activity took place with an accretionary setting on the margin of Rodinia rather than in the intracratonic position (e.g., Cawood and Korsch, 2008; Cawood et al., 2009, 2010, 2013; Wang et al., 2013b).

Acknowledgements

We would like to thank X-P Xia, T-P Peng, F-F Zhang and A-M Zhang for their help during fieldwork and dating analyses. We are grateful to Prof Guochun Zhao and two anonymous reviewers for their critical and constructive review on this paper. This study was supported by China Natural Science Foundation (41190073 and 41372198), National Basic Research Program of China (2014CB440901) and Natural Environment Research Council (grant NE/J021822/1).

References

Bao, Z.W., Wang, Q., Bai, G.D., Zhao, Z.H., Song, Y.W., Liu, X.M., 2008. Geochronology and geochemistry of the Fangcheng Neoproterozoic alkali-syenites in East Qinling orogen and its geodynamic implications. Chinese Science Bulletin 53, 2050–2061.

Barnes, S.J., Naldrett, A.J., Gorton, M.P., 1985. The origin of the fractionation of platinum-group elements in Terrestrial magmas. Chemical Geology 53, 303–323.

Cawood, P.A., Korsch, R.J., 2008. Assembling Australia: Proterozoic building of a continent. Precambrian Research 166, 1–35.

Cawood, P.A., Kröner, A., Collins, W.J., Kusky, T.M., Mooney, W.D., Windley, B.F., 2009. Accretionary orogens through Earth history. In: Cawood, P.A., Kröner, A. (Eds.), Earth Accretionary Systems in Space and Time. Geological Society of London Special Publication 318, pp. 1–36.

Cawood, P.A., Strachan, R., Cutts, K., Kinny, P.D., Hand, M., Pisarevsky, S., 2010. Neoproterozoic orogeny along the margin of Rodinia: Valhalla orogen, North Atlantic. Geology 38 (2), 99–102.

Cawood, P.A., Wang, Y.J., Xu, Y.J., Zhao, G.C., 2013. Locating South China in Rodinia and Gondwana: a fragment of greater India lithosphere? Geology 41 (8), 903–906.

Charvet, J., Shu, L.S., Shi, Y.S., Guo, L.Z., Faure, M., 1996. The building of south China: collision of Yangzi and Cathaysia blocks, problems and tentative answers. Journal of Southeast Asian Earth Sciences 13, 223–235.

Chen, D.G., Deloule, E., Chen, H., Xiao, Q.K., Wu, Y.B., 2003. Preliminary study of microscale zircon oxygen isotopes for Dabie-Sulu metamorphic rocks: ion probe in situ analyses. Chinese Science Bulletin 48 (16), 1670–1678.

Chen, J.F., Jahn, B.M., 1998. Crustal evolution of southeastern China: Nd and Sr isotopic evidence. Tectonophysics 284, 101–133.

Chen, M., Zheng, J.P., Sun, M., Zhao, J.H., 2013. Mid-Neoproterozoic crustal evolution of the northeastern Yangtze Block: evidence from the felsic-gneiss xenoliths hosted in the Donghai Cenozoic basalts. Journal of Asian Earth Sciences 66, 108–122.

Chen, R.X., Zheng, Y.F., Xie, L.W., 2010. Metamorphic growth and recrystallization of zircon: distinction by simultaneous in-situ analyses of trace elements, U–Th–Pb and Lu–Hf isotopes in zircons from eclogite-facies rocks in the Sulu orogen. Lithos 114, 132–154.

Chen, R.X., Zheng, Y.F., Zhao, Z.F., Tang, J., Wu, F.Y., Liu, X.M., 2007. Zircon U–Pb age and Hf isotope evidence for contrasting origin of bimodal protoliths for ultrahigh-pressure metamorphic rocks from the Chinese Continental Scientific Drilling project. Journal of Metamorphic Geology 25, 873–894.

Class, C., Miller, D.M., Goldstein, S.L., Langmuir, C.H., 2000. Distinguishing melt and fluid subduction components in Umnak Volcanics, Aleutian Arc. Geochemistry Geophysics Geosystems 1, 1004, http://dx.doi.org/10.1029/1999GC000010.

Dong, Y.P., Liu, X.M., Santosh, M., Chen, Q., Zhang, X.N., Li, W., He, D.F., Zhang, G.W., 2012. Neoproterozoic accretionary tectonics along the northwestern margin of the Yangtze Block, China: constraints from

zircon U–Pb geochronology and geochemistry. Precambrian Research 196, 247–274.
Dong, Y.P., Liu, X.M., Santosh, M., Zhang, X.N., Chen, Q., Yang, C., Yang, Z., 2011. Neoproterozoic subduction tectonics of the northwestern Yangtze Block in South China: constrains from zircon U–Pb geochronology and geochemistry of mafic intrusions in the Hannan Massif. Precambrian Research 189, 66–90.
Du, L.L., Geng, Y.S., Yang, C.H., Wang, X.S., Ren, L.D., Wang, Y.B., Yang, Z.S., 2007. New understanding on Kangding Group on western margin of Yangtze Block: evidence from geochemistry and chronology. Acta Geologica Sinica 81, 1562–1577 (in Chinese with English abstract).
Fan, W.M., Guo, F., Wang, Y.J., Zhang, M., 2004. Late Mesozoic volcanism in the northern Huaiyang tectono-magmatic belt, central China: partial melts from a lithospheric mantle with subducted continental crust relicts beneath the Dabie orogen? Chemical Geology 209, 27–48.
Fan, W.M., Wang, Y.J., Zhang, A.M., Zhang, F.F., Zhang, Y.Z., 2010. Permian arc-back-arc basin development along the Ailaoshan tectonic zone: geochemical, isotopic and geochronological evidence from the Mojiang volcanic rocks, Southwest China. Lithos 119, 553–568.
Ge, W.C., Li, X.H., Li, Z.X., Zhou, H.W., 2001. Mafic intrusions in Longsheng area: age and its geological implications. Chinese Journal of Geology 36, 112–118 (in Chinese with English abstract).
Gribble, R.F., Stern, R.J., Newman, S., Bloomer, S.H., O'Hearn, T., 1998. Chemical and isotopic composition of lavas from the Northern Mariana Trough: implications for magmagenesis in back-arc basins. Journal of Petrology 39, 125–154.
Hacker, B.R., Wallis, S.R., Ratschbacher, L., Grove, M., Gehrels, G., 2006. High-temperature geochronology constraints on the tectonic history and architecture of the ultrahigh-pressure Dabie-Sulu Orogen. Tectonics 25, TC5006, http://dx.doi.org/10.1029/2005TC001937.
Hawkesworth, C.J., Gallagher, K., Hergt, J.M., Mcdermott, F., 1993. Mantle and slab contributions in arc magmas. Annual Review of Earth and Planetary Sciences 21, 175–204.
Hawkins, J.W., 1995. The geology of the Lau Basin. In: Taylor, B. (Ed.), Back-arc Basins: Tectonics and Magmatism. Plenum Press, New York, pp. 63–138.
Hirose, K., 1997. Melting experiments on Iherzolite KLB-1 under hydrous conditions and generation of high-magnesian andesitic melts. Geology 25, 42–44.
Hieu, P.T., Chen, F., Zhu, X.Y., Wang, W., Nguyen, T.B.T., Bui, M.T., Nguyen, Q.L., 2009. Zircon U–Pb ages and Hf isotopic composition of the Posen granite in northwestern Vietnam. Acta Petrologica Sinica 25, 3141–3152 (in Chinese with English abstract).
Hieu, P.T., Chen, F., Me, L.T., Nguyen, T.B.T., Siebel, W., Lan, T.G., 2012. Zircon U–Pb ages and Hf isotopic compositions from the Sin Quyen Formation: the Precambrian crustal evolution of northwest Vietnam. International Geology Review 54, 1548–1561.
Hollings, P., Kerrich, R., 2004. Geochemical systematics of tholeiites from the 2.86 Ga Pickle Crow Assemblage, northwestern Ontario: arc basalts with positive and negative Nb–Hf anomalies. Precambrian Research 134, 1–20.
Hu, J., Qiu, J.S., Wang, R.C., Jiang, S.Y., Yu, J.H., Ni, P., 2007. Earliest response of the Neoproterozoic Rodinia break-up in the northeastern Yangtze craton: constraints from zircon U–Pb geochronology and Nd isotopes of the gneissic alkaline granites in Donghai area. Acta Petrologica Sinica 23, 1321–1333 (in Chinese with English Abstract).
Huang, X.L., Xu, Y.G., Li, X.H., Li, W.X., Lan, J.B., Zhang, H.H., Liu, Y.S., Wang, Y.B., Li, H.Y., Luo, Z.Y., Yang, Q.J., 2008. Petrogenesis and tectonic implications of Neoproterozoic, highly fractionated A-type granites from Mianning, South China. Precambrian Research 165, 190–204.
Kepezhinskas, P., Defant, M.J., Drummond, M.S., 1996. Progressive enrichment of island arc mantle by melt-peridotite interaction inferred from Kamchatka xenoliths. Geochimica et Cosmochimica Acta 60, 1217–1229.
Kepezhinskas, P., McDermott, F., Defant, M.J., Hochstaedter, A., Drummond, M.S., Hawkesworth, C.J., Koloskov, A., Maury, R.C., Bellon, H., 1997. Trace element and Sr–Nd–Pb isotopic constraints on a three-component model of Kamchatka arc petrogenesis. Geochimica et Cosmochimica Acta 61, 577–600.
Leat, P.T., Livermore, R.A., Millar, I.L., Pearce, J.A., 2000. Magma supply in back-arc spreading centre segment e2, east Scotia Ridge. Journal of Petrology 41, 845–866.
Leloup, P.H., Lacassin, R., Tapponnier, P., Scharer, U., Zhong, D.L., Liu, X.H., Zhang, L.S., Ji, S.C., Trinh, P.T., 1995. The Ailao Shan-Red River shear zone (Yunnan, China), Tertiary transform boundary of Indochina. Tectonophysics 251, 3–10.
Li, B.L., Dissertation for Doctoral Degree 2010. Thermal evolutional history and geochronological constrains on metamorphic-deformational zones in west Yunnan Province., pp. 57–59.
Li, W.X., Li, X.H., Li, Z.X., 2008b. Middle Neoproterozoic syn-rifting volcanic rocks in Guangfeng, South China: petrogenesis and tectonic significance. Geological Magazine 145, 475–489.
Li, W.X., Li, X.H., Li, Z.X., 2010. Ca. 850 Ma bimodal volcanic rocks in northeastern Jiangxi Province, South China: initial extension during the breakup of Rodinia? American Journal of Science 310, 951–980.
Li, X.H., 1999. U–Pb zircon ages of granites from the southern margin of the Yangtze Block: timing of Neoproterozoic Jinning: orogeny in SE China and implications for Rodinia Assembly. Precambrian Research 97, 43–57.
Li, X.H., Li, W.X., Li, Z.X., Liu, Y., 2008a. 850–790 Ma bimodal volcanic and intrusive rocks in northern Zhejiang, South China: a major episode of continental rift magmatism during the breakup of Rodinia. Lithos 102, 341–357.
Li, X.H., Li, W.X., Li, Z.X., Lo, C.H., Wang, J., Ye, M.F., Yang, Y.H., 2009b. Amalgamation between the Yangtze and Cathaysia Blocks in South China: constraints from SHRIMP U–Pb zircon ages, geochemistry and Nd–Hf isotopes of the Shuangxiwu volcanic rocks. Precambrian Research 174, 117–128.
Li, X.H., Li, Z.X., Ge, W.C., Zhou, H.W., Li, W.X., Liu, Y., Wingate, M.T.D., 2003b. Neoproterozoic granitoids in South China: crustal melting above a mantle plume at ca. 825 Ma? Precambrian Research 122, 45–83.
Li, X.H., Li, Z.X., Sinclair, J.A., Li, W.X., Carter, G., 2006. Revisiting the "Yanbian Terrane": implications for Neoproterozoic tectonic evolution of the western Yangtze Block, South China. Precambrian Research 151, 14–30.
Li, X.H., Li, Z.X., Zhou, H.W., Liu, Y., Kinny, P.D., 2002. U–Pb zircon geochronology, geochemistry and Nd isotopic study of Neoproterozoic bimodal volcanic rocks in the Kangdian Rift of South China: implications for the initial rifting of Rodinia. Precambrian Research 113, 135–154.
Li, X.H., Li, Z.X., Zhou, H.W., Liu, Y., Liang, X.R., Li, W.X., 2003c. SHRIMP U–Pb zircon age, geochemistry and Nd isotope of the Guandaoshan pluton in SW Sichuan: petrogenesis and tectonic significance. Science in China Series D: Earth Sciences 46, 73–83.
Li, X.H., Liu, Y., Li, Q.L., Guo, C.H., Chamberlain, K.R., 2009a. Precise determination of Phanerozoic zircon Pb/Pb age by multicollector SIMS without external standardization (vol 10, Q04010, 2009). Geochemistry Geophysics Geosystems, 10.
Li, Z.X., Li, X.H., Kinny, P.D., Wang, J., Zhang, S., Zhou, H., 2003a. Geochronology of Neoproterozoic syn-rift magmatism in the Yangtze Craton, South China and correlations with other continents: evidence for a mantle superplume that broke up Rodinia. Precambrian Research 122, 85–109.
Li, Z.X., Zhang, L.H., Powell, C.M., 1995. South China in Rodinia: part of the missing link between Australia-East Antarctica and Laurentia? Geology 23 (5), 407–410.
Liang, X.R., Wei, G.J., Li, X.H., Liu, Y., 2003. Precise measurement of $^{143}Nd/^{144}Nd$ and Sm/Nd ratios using multiple-collectors inductively coupled plasma-mass spectrometer (MC-ICPMS). Geochimica 32, 91–96 (in Chinese with English abstract).
Lin, T.H., Chung, S.L., Chiu, H.Y., Wu, F.Y., Yeh, M.W., Searle, M.P., Iizuka, Y., 2012. Zircon U–Pb and Hf isotope constraints from the Ailao Shan-Red River shear zone on the tectonic and crustal evolution of southwestern China. Chemical Geology 291, 23–37.
Ling, H.F., Shen, W.Z., Wang, R.C., Xu, S.J., 2001. Geochemical characteristics and genesis of Neoproterozoic granitoids in the northwestern margin of the Yangtze Block. Physics and Chemistry of the Earth Part A: Solid Earth and Geodesy 26, 805–819.
Ling, W.L., Gao, S., Zhang, B.R., Li, H.M., Liu, Y., Cheng, J.P., 2003. Neoproterozoic tectonic evolution of the northwestern Yangtze craton, South China: implications for amalgamation and break-up of the Rodinia Supercontinent. Precambrian Research 122, 111–140.
Liu, F., Wang, F., Liu, P., Liu, C., 2012. Multiple metamorphic events revealed by zircons from the Diancang Shan – Ailao Shan metamorphic complex, southeastern Tibetan Plateau. Gondwana Research, http://dx.doi.org/10.1016/j.gr.2012.10.016.
Liu, F.L., Gerdes, A., Zeng, L.S., Xue, H.M., 2008b. SHRIMP U–Pb dating, trace elements and the Lu–Hf isotope system of coesite-bearing zircon from amphibolite in the SW Sulu UHP terrane, eastern China. Geochimica et Cosmochimica Acta 72, 2973–3000.
Liu, F.L., Xu, Z.Q., Yang, J.S., Zhang, Z.M., Xue, H.M., Li, T.F., 2004. Geochemical characteristics and UHP metamorphism of granitic gneisses in the main drilling hole of Chinese Continental Scientific Drilling Project and its adjacent area. Acta Petrologica Sinica 20, 9–26 (in Chinese with English Abstract).
Liu, J.B., Zhang, L.M., 2013. Neoproterozoic low to negative $\delta^{18}O$ volcanic and intrusive rocks in the Qinling Mountains and their geological significance. Precambrian Research 230 (0), 138–167.
Liu, J.L., Wang, A.J., Cao, S.Y., Zou, Y.X., Tang, Y., Chen, Y., 2008a. Geochronology and tectonic implication of migmatites from Diancangshan, western Yunnan, China. Acta Petrologica Sinica 24, 413–420 (in Chinese with English abstract).
Lu, L.Z., 1989. The metamorphic series and crustal evolution of the basement of the Yangtze platform. Journal of Southeast Asian Earth Sciences 3, 293–301.
Ludwig, K.R., 2001. Users manual for Isoplot/Ex rev, 2. 49. Berkeley Geochronology Centre Special Publication, pp. 56.
Luhr, J.F., Haldar, D., 2006. Barren Island Volcano (NE Indian Ocean): island-arc high-alumina basalts produced by troctolite contamination. Journal of Volcanology and Geothermal Research 149, 177–212.
Ma, G., Li, H., Zhang, Z., 1984. An investigation of the age limits of the Sinian System in South China. Bulletin of the Yichang Institute of Geology Mineral Research 8, 1–29 (in Chinese with English Abstract).
Ma, G., Zhang, Z., Li, H., Chen, P., Huang, Z., 1989. A geochronostratigraphical study of the Sinian System in Yangtze Platform. Bulletin of the Yichang Institute of Geology Mineral Research 14, 83–124 (in Chinese with English Abstract).
Macdonald, R., Hawkesworth, C.J., Heath, E., 2000. The Lesser Antilles volcanic chain: a study in arc magmatism. Earth Science Reviews 49, 1–76.
Pearce, J.A., 1983. In: Hawkesworth, C.J., Norry, M.J. (Eds.), Continental basalts and mantle xenolith (Shaiva Geology Series). Shiva, pp. 230–249.
Pearce, J.A., 2008. Geochemical fingerprinting of oceanic basalts with applications to ophiolite classification and the search for Archean oceanic crust. Lithos 100, 14–48.
Pearce, J.A., Peate, D.W., 1995. Tectonic implications of the composition of volcanic arc magmas. Annual Review of Earth and Planetary Sciences 23, 251–285.
Pearce, J.A., Stern, R.J., 2006. The origin of back-arc basin magmas: trace element and isotope perspectives. AGU Geophysical Monograph Series 166, 63–86.
Pei, X.Z., Li, Z.C., Ding, S.P., Li, R.B., Feng, J.Y., Sun, Y., Zhang, Y.F., Liu, Z.Q., 2009. Neoproterozoic Jiaoziding peraluminous granite in the northwest margin of Yangtze Block: zircon SHRIMP U–Pb age and geochemistry, and their tectonic significance. Earth Science Frontiers 16, 231–249 (in Chinese with English Abstract).
Qi, L., Jing, H., Gregoire, D.C., 2000. Determination of trace elements in granites by inductively coupled plasma mass spectrometry. Talanta 51, 507–513.

Qi, X.X., Zeng, L.S., Zhu, L.H., Hu, Z.C., Hou, K.J., 2012. Zircon U–Pb and Lu–Hf isotopic systematics of the Daping plutonic rocks: implications for the Neoproterozoic tectonic evolution of the northeastern margin of the Indochina block, Southwest China. Gondwana Research 21, 180–193.
Qin, X.F., Pan, Y.M., Li, L., Li, R.S., Zhou, F.S., Hu, G.A., Zhong, F.Y., 2006. Zircon SHRIMP U–Pb geochronology of the Yunkai metamorphic complex in southeastern Guangxi, China. Geological Bulletin of China 25 (5), 553–559.
Qiu, Y.M., Gao, S., McNaughton, N.J., Groves, D.I., Ling, W.L., 2000. First evidence of >3.2 Ga continental crust in the Yangtze Craton of South China and its implications for Archean crustal evolution and Phanerozoic tectonics. Geology 28 (1), 11–14.
Roger, F., Calassou, S., 1997. U–Pb geochronology on zircon and isotope geochemistry (Pb, Sr and Nd) of the basement in the Songpan-Garze fold belt (China). Comptes Rendus de l Academie des Sciences Serie ii Fascicule A: Sciences de la Terre et des Planetes 324, 819–826.
Rolland, Y., Galoyan, G., Bosch, D., Sosson, M., Corsini, M., Fornari, M., Verati, C., 2009. Jurassic back-arc and Cretaceous hot-spot series In the Armenian ophiolites: implications for the obduction process. Lithos 112, 163–187.
Sajona, F.G., Maury, R.C., Bellon, H., Cotten, J., Defant, M., 1996. High field strength element enrichment of Pliocene-Pleistocene Island arc basalts, Zamboanga Peninsula, western Mindanao (Philippines). Journal of Petrology 37, 693–726.
Sajona, F.G., Maury, R.C., Bellon, H., Cotten, J., Defant, M.J., Pubellier, M., 1993. Initiation of subduction and the generation of slab melts in western and eastern Mindanao, Philippines. Geology 21, 1007–1010.
Sandeman, H.A., Hanmer, S., Tella, S., Armitage, A.A., Davis, W.J., Ryan, J.J., 2006. Petrogenesis of Neoarchaean volcanic rocks of the MacQuoid supracrustal belt: a back-arc setting for the northwestern Hearne subdomain, western Churchill Province, Canada. Precambrian Research 144, 140–165.
Shinjo, R., Chung, S.L., Kato, Y., Kimura, M., 1999. Geochemical and Sr–Nd isotopic characteristics of volcanic rocks from the Okinawa Trough and Ryukyu Arc: implications for the evolution of a young, intracontinental back arc basin. Journal of Geophysical Research: Solid Earth 104, 10591–10608.
Shu, L.S., Deng, P., Yu, J.H., Wang, Y.B., Jiang, S.Y., 2008. The age and tectonic environment of the rhyolitic rocks on the western side of Wuyi Mountain, South China. Science in China Series D: Earth Sciences 51 (8), 1053–1063.
Shu, L.S., Faure, M., Yu, J.H., Jahn, B.M., 2011. Geochronological and geochemical features of the Cathaysia block (South China): new evidence for the Neoproterozoic breakup of Rodinia. Precambrian Research 187 (3–4), 263–276.
Sinclair, J.A., Honours Thesis 2001. Petrology, geochemistry, and geochronology of the "Yanbian ophiolite suite", South China: implications for the western extension of the Sibao Orogen. The University of Western Australia, Perth, pp. 69 (plus appendixes).
Stacey, J.S., Kramers, J.D., 1975. Approximation of terrestrial lead isotope evolution by a 2-stage model. Earth and Planetary Science Letters 26, 207–221.
Stern, R.J., 2002. Subduction zones. Reviews of Geophysics 40, 4.
Sun, S.S., McDonough, W.F., 1989. Chemical and isotopic systematics of oceanic basalts: implications for mantle composition and processes. Geological Society, London, Special Publications 42, 313–345.
Tapponnier, P., Lacassin, R., Leloup, P.H., Scharer, U., Zhong, D.L., Wu, H.W., Liu, X.H., Ji, S.C., Zhang, L.S., Zhong, J.Y., 1990. The Ailao Shan-Red River metamorphic belt: Tertiary left-lateral shear between Indochina and South China. Nature 343, 431–437.
Upton, B.G.J., Emeleus, C.H., 1987. Mid-Proterozoic alkaline magmatism in southern Greenland: the Gardar province. In: Fitton, J.G., Upton, B.G.J. (Eds.), Alkaline Igneous Rocks Geological Society Special Publication 30, 449–471.
Viruete, J.E., Contreras, F., Stein, G., Urien, P., Joubert, M., Perez-Estaun, A., Friedman, R., Ullrich, T., 2007. Magmatic relationships and ages between adakites, magnesian andesites and Nb-enriched basalt-andesites from Hispaniola: record of a major change in the Caribbean island arc magma sources. Lithos 99, 151–177.
Wang, P.L., Lo, C.H., Lan, C.Y., Chung, S.L., Lee, T.Y., Tran, N.N., Sano, Y., 2011a. Thermochronology of the PoSen complex, northern Vietnam: implications for tectonic evolution in SE Asia. Journal of Asian Earth Sciences 40, 1044–1055.
Wang, Q., Wyman, D.A., Li, Z.X., Bao, Z.W., Zhao, Z.H., Wang, Y.X., Jian, P., Yang, Y.H., Chen, L.L., 2010. Petrology, geochronology and geochemistry of ca 780 Ma A-type granites in South China: petrogenesis and implications for crustal growth during the breakup of the supercontinent Rodinia. Precambrian Research 178, 185–208.
Wang, X.C., Li, X.H., Li, W.X., Li, Z.X., 2007b. Ca, 825 Ma komatiitic basalts in South China: first evidence for >1500 °C mantle melts by a Rodinian mantle plume. Geology 35, 1103–1106.
Wang, X.C., Li, X.H., Li, W.X., Li, Z.X., Liu, Y., Yang, Y.H., Liang, X.R., Tu, X.L., 2008c. The Bikou basalts in the northwestern Yangtze block, South China: remnants of 820–810 Ma continental flood basalts? Geological Society of America Bulletin 120, 1478–1492.
Wang, X.L., Shu, L.S., Xing, G.F., Zhou, J.C., Tang, M., Shu, X.J., Qi, L., Hu, Y.H., 2012a. Post-orogenic extension in the eastern part of the Jiangnan orogen: evidence from ca 800–760 Ma volcanic rocks. Precambrian Research 222, 404–423.
Wang, X.L., Zhao, G.C., Zhou, J.C., Liu, Y.S., Hu, J., 2008a. Geochronology and Hf isotopes of zircon from volcanic rocks of the Shuangqiaoshan Group, South China: implications for the Neoproterozoic tectonic evolution of the eastern Jiangnan orogen. Gondwana Research 14, 355–367.
Wang, X.L., Zhou, J.C., Qi, J.S., Jiang, S.Y., Shi, Y.R., 2008b. Geochronology and geochemistry of Neoproterozoic mafic rocks from western Hunan, South China: implications for petrogenesis and post-orogenic extension. Geological Magazine 145, 215–233.
Wang, X.L., Zhou, J.C., Qiu, J.S., Zhang, W.L., Liu, X.M., Zhang, G.L., 2006. LA-ICP-MS U–Pb zircon geochronology of the Neoproterozoic igneous rocks from Northern Guangxi, South China: implications for tectonic evolution. Precambrian Research 145, 111–130.
Wang, Y.J., Fan, W.M., Zhao, G.C., Ji, S.C., Peng, T.P., 2007a. Zircon U–Pb geochronology of gneissic rocks in the Yunkai massif and its implications on the Caledonian event in the South China Block. Gondwana Research 12, 404–416.
Wang, Y.J., Fang, W.M., Zhang, Y.H., Guo, F., Zhang, H.F., Peng, T.P., 2004. Geochemical $^{40}Ar/^{39}Ar$ geochronological and Sr–Nd isotopic constraints on the origin of Paleoproterozoic mafic dikes from the southern Taihang Mountains and implications for the ca, 1800 Ma event of the North China Craton. Precambrian Research 135, 55–77.
Wang, Y.J., Wu, C.M., Zhang, A.M., Fan, W.M., Zhang, Y.H., Zhang, Y.Z., Peng, T.P., Yin, C.Q., 2012b. Kwangsian and Indosinian reworking of the eastern South China Block: constraints on zircon U–Pb geochronology and metamorphism of amphibolites and granulites. Lithos 150, 227–242.
Wang, Y.J., Zhang, A.M., Fan, W.M., Zhang, Y.H., Zhang, Y.Z., 2013a. Origin of paleosubduction-modified mantle for Silurian gabbro in the Cathaysia Block: geochronological and geochemical evidence. Lithos 160, 37–54.
Wang, Y.J., Zhang, A.M., Cawood, P.A., Fan, W.M., Xu, J.F., Zhang, G.W., Zhang, Y.Z., 2013b. Geochronological, geochemical and Nd–Hf–Os isotopic fingerprinting of an early Neoproterozoic arc–back-arc system in South China and its accretionary assembly along the margin of Rodinia. Precambrian Research 231, 343–371.
Wang, Y.J., Zhang, A.M., Fan, W.M., Zhao, G.C., Zhang, G.W., Zhang, Y.Z., Zhang, F.F., Li, S.Z., 2011. Kwangsian crustal anatexis within the eastern South China Block: geochemical, zircon U–Pb geochronological and Hf isotopic fingerprints from the gneissoid granites of Wugong and Wuyi–Yunkai Domains. Lithos 127, 239–260.
Wang, Y.J., Zhao, G.C., Fan, W.M., Peng, T.P., Sun, L.H., Xia, X.P., 2007c. LA-ICP-MS U–Pb zircon geochronology and geochemistry of Paleoproterozoic mafic dykes from western Shandong Province: implications for back-arc basin magmatism in the Eastern Block, North China Craton. Precambrian Research 154, 107–124.
Wiedenbeck, M., Alle, P., Corfu, F., Griffin, W.L., Meier, M., Oberli, F., Vonquadt, A., Roddick, J.C., Speigel, W., 1995. 3 natural zircon standards for U–Th–Pb, Lu–Hf, trace-element and REE analyses. Geostandard Newsletter 19, 1–23.
Winchester, J.A., Floyd, P.A., 1977. Geochemical discrimination of different magma series and their differentiation products using immobile elements. Chemical Geology 20, 325–343.
Woodhead, J., Eggins, S., Gamble, J., 1993. High-field strength and transition element systematics in island-arc and back-arc basin basalts: evidence for multiphase melt extraction and a depleted mantle wedge. Earth and Planetary Science Letters 114 (4), 491–504.
Wu, G.G., Yu, X.Q., Di, Y.J., Zhang, D., 2010. Neoproterozoic tectonic setting of southeast China: new constraints from SHRIMP U–Pb zircon ages and petrographic studies on the Mamianshan Group. Acta Geologica Sinica: English Edition 84, 333–344.
Xia, L.Q., Xia, Z.C., Ma, Z.P., Xu, X.Y., Li, X.M., 2009. Petrogenesis of volcanic rocks from Xixiang Group in middle part of South Qinling Mountains. Northwestern Geology 42, 1–37 (in Chinese with English Abstract).
Xia, X.P., Sun, M., Zhao, G.C., Li, H.M., Zhou, M.F., 2004. Spot zircon U–Pb isotope analysis by ICP-MS coupled with a frequency quintupled (213 nm) Nd-YAG laser system. Geochemical Journal 38, 191–200.
Xu, H., Yang, T., Liu, F., Liou, J.G., 2001. Multi age-time evolution of granite gneisses-granite in the southern Sulu HP–UHP metamorphic belt. Acta Geologica Sinica 75, 371–378 (in Chinese with English Abstract).
Xu, Z.Q., Liu, F.L., Qi, X.X., Zhang, Z.M., Yang, J.S., Zeng, L.S., Liang, F.H., 2006. Record for Rodinia suppercontinent breakup event in the south Sulu ultra-high pressure metamorphic terrane. Acta Petrologica Sinica 22, 1745–1760 (in Chinese with English Abstract).
Xue, H.M., Ma, F., Song, Y.Q., Xie, Y.P., 2010. Geochronology and geochemistry of the Neoproterozoic granitoid association from eastern segment of the Jiangnan orogen, China: constraints on the timing and process of amalgamation between the Yangtze and Cathaysia blocks. Acta Petrologica Sinica 26, 3215–3244 (in Chinese with English abstract).
Yan, Q.R., Hanson, A.D., Wang, Z.Q., Druschke, P.A., Yan, Z., Wang, T., Liu, D.Y., Song, B., Pan, P., Zhou, H., Jiang, C.F., 2004. Neoproterozoic subduction and rifting on the northern margin of the Yangtze Plate, China: implications for Rodinia reconstruction. International Geology Review 46, 817–832.
Ye, M.F., Li, X.H., Li, W.X., Liu, Y., Li, Z.X., 2007. SHRIMP zircon U–Pb geochronological and whole-rock geochemical evidence for an early Neoproterozoic Sibaoian magmatic arc along the southeastern margin of the Yangtze Block. Gondwana Research 12, 144–156.
Yin, C.Q., Lin, S.F., Davis, D.W., Xing, G.F., Davis, W.J., Cheng, G.H., Xiao, W.J., Li, L.M., 2013. Tectonic evolution of the southeastern margin of the Yangtze Block: constraints from SHRIMP U–Pb and LA-ICP-MS Hf isotopic studies of zircon from the eastern Jiangnan Orogenic Belt and implications for the tectonic interpretation of South China. Precambrian Research 236, 145–156.
Yunnan BGMR (Bureau of geology and mineral resources of Yunnan), 1983. Geological Map of Yunnan, scale 1:1 000000. Kumming (in Chinese with English abstract).
Zeng, W., Zhou, H.W., Zhong, Z.Q., Zeng, Z.G., Li, H.M., 2005. Single zircon U–Pb ages and their tectonic implications of Neoproterozoic magmatic rocks in southeastern Guizhou, China. Geochimica 34, 548–556 (in Chinese with English abstract).
Zhang, A.M., Wang, Y.J., Fan, W.M., Zhang, Y.Z., Yang, J., 2012a. Earliest Neoproterozoic (ca. 1.0 Ga) arc-back-arc basin nature along the northern Yunkai Domain of the Cathaysia Block: geochronological and geochemical evidence from the metabasite. Precambrian Research 220, 217–233.

Zhang, C.L., Li, H.K., Santosh, M., 2013a. Revisiting the tectonic evolution of South China: interaction between the Rodinia superplume and plate subduction? Terra Nova 25, 212–220.
Zhang, C.L., Liu, L., Zhang, G.W., Wang, T., Chen, D.L., Yuan, H.L., Liu, X.M., Yan, Y.X., 2004. Determination of Neoproterozoic post-collisional granites in the North Qinling Mountains and its tectonic significance. Earth Science Frontier 11, 33–42 (in Chinese with English abstract).
Zhang, G.W., Yu, Z.P., Dong, Y.P., Yao, A.P., 2000. On Precambrian framework and evolution of the Qinling belt. Acta Petrologica Sinica 16, 11–21.
Zhang, S.B., Wu, R.X., Zheng, Y.F., 2012c. Neoproterozoic continental accretion in South China: geochemical evidence from the Fuchuan ophiolite in the Jiangnan orogen. Precambrian Research 220, 45–64.
Zhang, Y.Z., Wang, Y.J., Fan, W.M., Zhang, A.M., Ma, L.Y., 2012b. Geochronological and geochemical constraints on the metasomatised source for the Neoproterozoic (similar to 825 Ma) high-mg volcanic rocks from the Cangshuipu area (Hunan Province) along the Jiangnan domain and their tectonic implications. Precambrian Research 220, 139–157.
Zhang, Y.Z., Wang, Y.J., Geng, H.Y., Zhang, Y.H., Fan, W.M., Zhong, H., 2013b. Early Neoproterozoic (similar to 850 Ma) back-arc basin in the Central Jiangnan Orogen (Eastern South China): geochronological and petrogenetic constraints from meta-basalts. Precambrian Research 231, 325–342.
Zhang, Z.Q., Zhang, G.W., Liu, D.Y., Wang, Z.Q., Tan, S.H., Wang, J.H., 2006. Isotopic Geochoronology and Geochemistry of Ophiolites, Granites and Clastic Sedimentary Rocks in the Qinling-Dabie Orogenic Belt. Geological Publishing House, Beijing (in Chinese).
Zhang, Z.L., Yuan, H.H., Nan, Y., 1998. Whole grain zircon evaporation for age of Luoyu formation, Yunkai Group. Mineralogy Petrology 18, 85–90 (in Chinese with English abstract).
Zhao, F.Q., Zhao, W.P., Zuo, Y.C., Li, Z.H., Xue, K.Q., 2006. U–Pb geochronology of Neoproterozoic magmatic rocks in Hanzhong, southern Shaanxi, China. Geological Bulletin of China 25, 383–388 (in Chinese with English abstract).
Zhao, G.C., Cawood, P.A., 1999. Tectonothermal evolution of the Mayuan assemblage in the Cathaysia Block: implications for Neoproterozoic collision-related assembly of the South China craton. American Journal of Science 299, 309–339.
Zhao, G.C., Cawood, P.A., 2012. Precambrian geology of China. Precambrian Research 222, 13–54.
Zhao, G.C., Guo, J.H., 2012. Precambrian geology of China: preface. Precambrian Research 222, 1–12.
Zhao, J.H., Zhou, M.F., Yan, D.P., Zheng, J.P., Li, J.W., 2011. Reappraisal of the ages of Neoproterozoic strata in South China: no connection with the Grenvillian orogeny. Geology 39, 299–302.
Zhao, J.H., Zhou, M.F., Zheng, J.P., 2013. Neoproterozoic high-K granites produced by melting of newly formed mafic crust in the Huangling region, South China. Precambrian Research 233, 97–107.
Zhao, J.H., Zhou, M.F., 2007. Geochemistry of Neoproterozoic mafic intrusions in the Panzhihua district (Sichuan Province, SW China): implications for subduction-related metasomatism in the upper mantle. Precambrian Research 152, 27–47.
Zhao, J.H., Zhou, M.F., 2008. Neoproterozoic adakitic plutons in the northern margin of the Yangtze Block, China: partial melting of a thickened lower crust and implications for secular crustal evolution. Lithos 104, 231–248.
Zhao, J.H., Zhou, M.F., 2009. Secular evolution of the Neoproterozoic lithospheric mantle underneath the northern margin of the Yangtze Block, South China. Lithos 107, 152–168.
Zhao, J.H., Zhou, M.F., Zheng, J.P., Fang, S.M., 2010. Neoproterozoic crustal growth and reworking of the Northwestern Yangtze Block: constraints from the Xixiang dioritic intrusion, South China. Lithos 120, 439–452.
Zhao, X.F., Zhou, M.F., Li, J.W., Wu, F.Y., 2008. Association of Neoproterozoic A- and I-type granites in South China: implications for generation of A-type granites in a subduction-related environment. Chemical Geology 257, 1–15.
Zheng, Y.F., Wu, R.X., Wu, Y.B., Zhang, S.B., Yuan, H.L., Wu, F.Y., 2008. Rift melting of juvenile arc-derived crust: geochemical evidence from Neoproterozoic volcanic and granitic rocks in the Jiangnan Orogen, South China. Precambrian Research 163, 351–383.
Zhong, D.L., 1998. Paleotethysides in Western Yunnan and Sichuan, China. Science Press, Beijing, pp. 9–215.
Zhou, J.C., Wang, X.L., Qiu, J.S., 2009. Geochronology of Neoproterozoic mafic rocks and sandstones from northeastern Guizhou, South China: coeval arc magmatism and sedimentation. Precambrian Research 170, 27–42.
Zhou, M.F., Kennedy, A.K., Sun, M., Malpas, J., Lesher, C.M., 2002a. Neoproterozoic arc-related mafic intrusions along the northern margin of South China: implications for the accretion of Rodinia. Journal of Geology 110, 611–618.
Zhou, M.F., Ma, Y.X., Yan, D.P., Xia, X.P., Zhao, J.H., Sun, M., 2006b. The Yanbian terrane (Southern Sichuan Province, SW China): a Neoproterozoic arc assemblage in the western margin of the Yangtze block. Precambrian Research 144, 19–38.
Zhou, M.F., Yan, D.P., Kennedy, A.K., Li, Y.Q., Ding, J., 2002b. SHRIMP U–Pb zircon geochronological and geochemical evidence for Neoproterozoic arc-magmatism along the western margin of the Yangtze Block, South China. Earth and Planetary Science Letters 196, 51–67.
Zhou, M.F., Yan, D.P., Wang, C.L., Qi, L., Kennedy, A., 2006a. Subduction-related origin of the 750 Ma Xuelongbao adakitic complex (Sichuan Province China): implications for the tectonic setting of the giant Neoproterozoic magmatic event in South China. Earth and Planetary Science Letters 248, 286–300.
Zhu, W.G., Zhong, H., Deng, H.L., Wilson, A.H., Liu, B.G., Li, C.Y., Qin, Y., 2006. SHRIMP zircon U–Pb age, geochemistry, and Nd–Sr isotopes of the Gaojiacun mafic-ultramafic intrusive complex, Southwest China. International Geology Review 48, 650–668.
Zhu, W.G., Zhong, H., Li, X.H., Deng, H.L., He, D.F., Wu, K.W., Bai, Z.J., 2008. SHRIMP zircon U–Pb geochronology, elemental, and Nd isotopic geochemistry of the Neoproterozoic mafic dykes in the Yanbian area, SW China. Precambrian Research 164, 66–85.